JCB Journal of Cell Biology

ARTICLE

The Wave complex controls epidermal morphogenesis and proliferation by suppressing Wnt–Sox9 signaling

Jonathan Cohen, Shaul Raviv, Orit Adir, Krishnanand Padmanabhan, Arad Soffer, and Chen Luxenburg

Development of the skin epidermis requires tight spatiotemporal control over the activity of several signaling pathways; however, the mechanisms that orchestrate these events remain poorly understood. Here, we identify a key role for the Wave complex proteins ABI1 and Wave2 in regulating signals that control epidermal shape and growth. In utero RNAi-mediated silencing of *Abi1* or *Wasf2* induced cellular hyperproliferation and defects in architecture of the interfollicular epidermis (IFE) and delayed hair follicle growth. Unexpectedly, SOX9, a hair follicle growth regulator, was aberrantly expressed throughout the IFE of the mutant embryos, and its forced overexpression mimicked the Wave complex loss-of-function phenotype. Moreover, Wnt signaling, which regulates SOX9$^+$ cell specification, was up-regulated in Wave complex loss-of-function IFE. Importantly, we show that the Wave complex regulates filamentous actin content and that a decrease in actin levels is sufficient to elevate Wnt/β-catenin signaling. Our results identify a novel role for Wave complex– and actin-regulated signaling via Wnt and SOX9 in skin development.

Introduction

The actin cytoskeleton is a complex cellular structure that regulates numerous biological processes and has well-established roles in the structural organization and mechanical function of the cell. Studies over the past several decades have demonstrated that the actin cytoskeleton also plays a major regulatory role in controlling signal transduction, gene expression, and cell fate determination (Pollard and Cooper, 2009; Olson and Nordheim, 2010; Bisi et al., 2013; Zaidel-Bar et al., 2015; Luxenburg and Geiger, 2017). However, there are large gaps in our understanding of the molecular mechanisms by which the actin cytoskeleton contributes to these processes.

The developing mouse skin epidermis is an excellent model system for addressing this knowledge gap and determining how the actin cytoskeleton functions in a complex, physiologically relevant mammalian system. The actin cytoskeleton regulates epidermal morphogenesis by controlling structural features such as basement membrane (BM) assembly and cell adhesion, polarity, and shape (Luxenburg et al., 2015; Dor-On et al., 2017; Rübsam et al., 2017; Miroshnikova et al., 2018). In addition, regulators of the actin cytoskeleton and actin-binding proteins also mediate key signaling events in the epidermis. For instance, the two small GTPases Rac1 and Cdc42 regulate c-Myc activity (Benitah et al., 2005) and Wnt signaling (Wu et al., 2006), respectively, both of which are pivotal regulators in the epidermis. Yap signaling, which affects epidermal proliferation, differentiation, and morphogenesis, is also regulated by major actin-binding proteins, including α-catenin (Schlegelmilch et al., 2011; Silvis et al., 2011) and components of the Arp2/3 complex (Zhou et al., 2013).

The Arp2/3 complex nucleates F-actin and generates branched networks of actin fibers (Machesky et al., 1994; Welch et al., 1997; Winter et al., 1997; Machesky and Gould, 1999). In the developing mouse epidermis, loss of Arp2/3 activity negatively affects the establishment of barrier function due to defects in differentiation and formation of the granular layer and its tight junctions (Zhou et al., 2013). In the adult, Arp2/3 loss of function gives rise to psoriasis-like disease (van der Kammen et al., 2017)

Activation of the Arp2/3 complex requires nucleation-promoting factors (NPFs), which are a large and diverse group of proteins that ensure tight spatiotemporal regulation of Arp2/3 activity (Campellone and Welch, 2010; Rotty et al., 2013; Alekhina et al., 2017). Neuronal Wiskott–Aldrich syndrome protein (nWASP) is an NPF present in many tissues, including the epidermis. Notably, loss of nWASP function gives rise to

Department of Cell and Developmental Biology, Sackler Faculty of Medicine, Tel Aviv University, Tel Aviv, Israel.

Correspondence to Chen Luxenburg: lux@tauex.tau.ac.il.

alopecia (Lefever et al., 2010; Lyubimova et al., 2010; Kalailingam et al., 2017) and interfollicular epidermis (IFE) hyperproliferation (Lyubimova et al., 2010; Kalailingam et al., 2017) due to inflammation (Kalailingam et al., 2017).

The WASP-family verprolin-homologous (Wave) proteins are also NPFs that regulate cell structure and function. Wave proteins function as part of a heteropentameric Wave complex, which is composed of one of three isoforms of Wave (1–3), ABI (1–3), SRA1, NAP1, and BRK1 (Miki et al., 1998; Machesky et al., 1999; Stradal et al., 2004). Loss of ABI1 function in cultured nonmuscle cells demonstrated that it is essential for Wave complex stability and plays a role in actin polymerization and remodeling, cell spreading, migration, adhesion, and cytokinesis (Innocenti et al., 2004; Pollitt and Insall, 2008; Kotula, 2012). ABI1 was also shown to be essential for smooth muscle cell contractility (Wang et al., 2013). *Abi1* knockout (KO) mice exhibit defects in heart and brain development and die at embryonic day 11.5 (E11.5; Dubielecka et al., 2011; Ring et al., 2011). Conditional deletion of *Abi1* in the mouse prostate gives rise to defects in cell adhesion and to prostatic neoplasia (Xiong et al., 2012). However, the role of ABI1 or the Wave complex in the epidermis is unknown.

Here, we investigated the roles of *Abi1* and the Wave2-encoding gene *Wasf2* in the developing mouse epidermis by RNAi-mediated gene silencing in utero. We demonstrate that the Wave complex regulates IFE architecture and proliferation and hair follicle (HF) morphogenesis. In the absence of ABI1 or Wave2, the transcription factor SOX9, which is usually restricted to HFs in the epidermis, is ectopically expressed throughout the IFE, and forced overexpression of SOX9 in the developing IFE mimics the Wave complex loss-of-function phenotype. Wnt signaling, which regulates SOX9 expression, is also up-regulated in the IFE of embryos with Wave complex loss of function. These observations delineate a novel role for the Wave complex in regulating Wnt signaling and identify a new mechanism that links tissue shape and growth during epidermal development.

Results

Cytoskeletal defects in the developing epidermis after in utero silencing of *Abi1*

To understand the function of ABI1 in the developing mouse epidermis, we first examined its localization by injecting the embryonic sacs of E9 CD1 mouse embryos with lentiviruses harboring GFP-tagged *ABI1* (*ABI1-GFP*; Innocenti et al., 2004; derived by hPGK promoter). Analysis of dorsal skin sections from embryos at E16.5 showed that ABI1-GFP was present in the periphery of keratinocytes in all epidermal layers (Fig. 1 A). Immunostaining of another Wave complex protein, Wave2, and the Arp2/3 complex protein Arp3 showed similar patterns of expression (Fig. 1 A).

To study the function of *Abi1* in skin development, we first identified two *Abi1*-specific short hairpin RNAs (shRNAs), termed *Abi1-2082* and *Abi1-488*, which depleted *Abi1* mRNA levels in primary mouse keratinocytes by 74 ± 6% and 66 ± 6%, respectively (Fig. 1 B), and reduced ABI1 protein expression by comparable amounts (Fig. 1 C). We injected the embryonic sacs of E9 wild-type mouse embryos in utero with lentiviruses expressing *Abi1-2082*, *Abi1-488*, or scrambled shRNA (*Ctrl*) together with a GFP-tagged histone 2B reporter (H2B-GFP) to identify transduced cells. Mosaic tissue sections were analyzed to allow the uninfected (GFP^-) tissue patches to serve as an internal control for the effects of *Abi1* knockdown (KD) in adjacent GFP^+ patches. *Abi1* KD epidermis showed a marked reduction in Wave2 staining in patches containing infected, but not uninfected, cells (Fig. 1 D). In contrast, Arp3 localization and expression level were unaffected by *Abi1* KD (Fig. 1 E). Western blot analysis of shRNA-infected primary mouse keratinocytes confirmed that Wave2, but not Arp3, was down-regulated in *Abi1*-depleted cells (Fig. 1 F). Thus, *Abi1* KD affects the expression of ABI1 and Wave2 proteins without affecting Arp3 levels.

Since the major function of the Wave complex is to enhance Arp2/3-mediated actin polymerization, we determined whether *Abi1* depletion affects the F-actin content of developing epidermis. Embryos were injected with *shScr;H2B-GFP* (Ctrl) or *shAbi1; H2B-GFP* lentiviruses on E9, and at E16.5, dorsal skin sections were stained with fluorescent phalloidin, which binds specifically to F-actin. The fluorescence intensity ratio between GFP^+ and adjacent GFP^- tissue sections was calculated. Notably, *shAbi1*-expressing cells showed a significant decrease (19.6 ± 1.5%) in phalloidin staining intensity compared with *shScr*-expressing cells (Fig. 1, G and H). Thus, *Abi1* depletion compromises actin polymerization. In agreement with the data above, we also noted that the eyes of *shScr*-injected (Ctrl) embryos were closed at E16.5, whereas those of *Abi1* KD embryos were open (Fig. 1 I). This is consistent with the known major role of the actin cytoskeleton in eyelid closure (Heller et al., 2014). Taken together, these data indicate that ABI1 is an essential component of the Wave complex and regulates Wave2 levels and F-actin content in the developing mouse epidermis.

Abi1 depletion affects basal layer expansion and IFE morphology but not cell differentiation

Given the pivotal role of Arp2/3 (Zhou et al., 2013) and the actin cytoskeleton (Luxenburg et al., 2011) in IFE differentiation, we next examined the effects of *Abi1* depletion on expression of the epidermal cell markers keratin 14 (K14, basal layer), K10 (suprabasal layers), and filaggrin (granular layer). Immunostaining of dorsal skin on E16.5 revealed that IFE from control embryos was relatively flat, whereas *Abi1* KD IFE exhibited an abnormal curved and irregular shape (Fig. 2, A–C). Moreover, control IFE showed uniform K14 staining in a single basal layer, K10 staining in all suprabasal layers, and filaggrin staining restricted to the most apical layers (Fig. 2, A–C). In contrast, IFE from *Abi1* KD embryos showed $K14^+$ cells in multiple layers throughout the skin, with massive aggregates of up to 15 $K14^+$ cell layers in many regions (Fig. 2 A). Similarly, K10 staining in *Abi1* KD epidermis was not uniform, with all suprabasal cells stained in some regions and no staining in five to six cell layers in other regions (Fig. 2 B). Finally, filaggrin expression appeared to be unaffected by *Abi1* KD, since staining was readily detected in the most apical layers and was comparable in the KD and control embryos (Fig. 2 C).

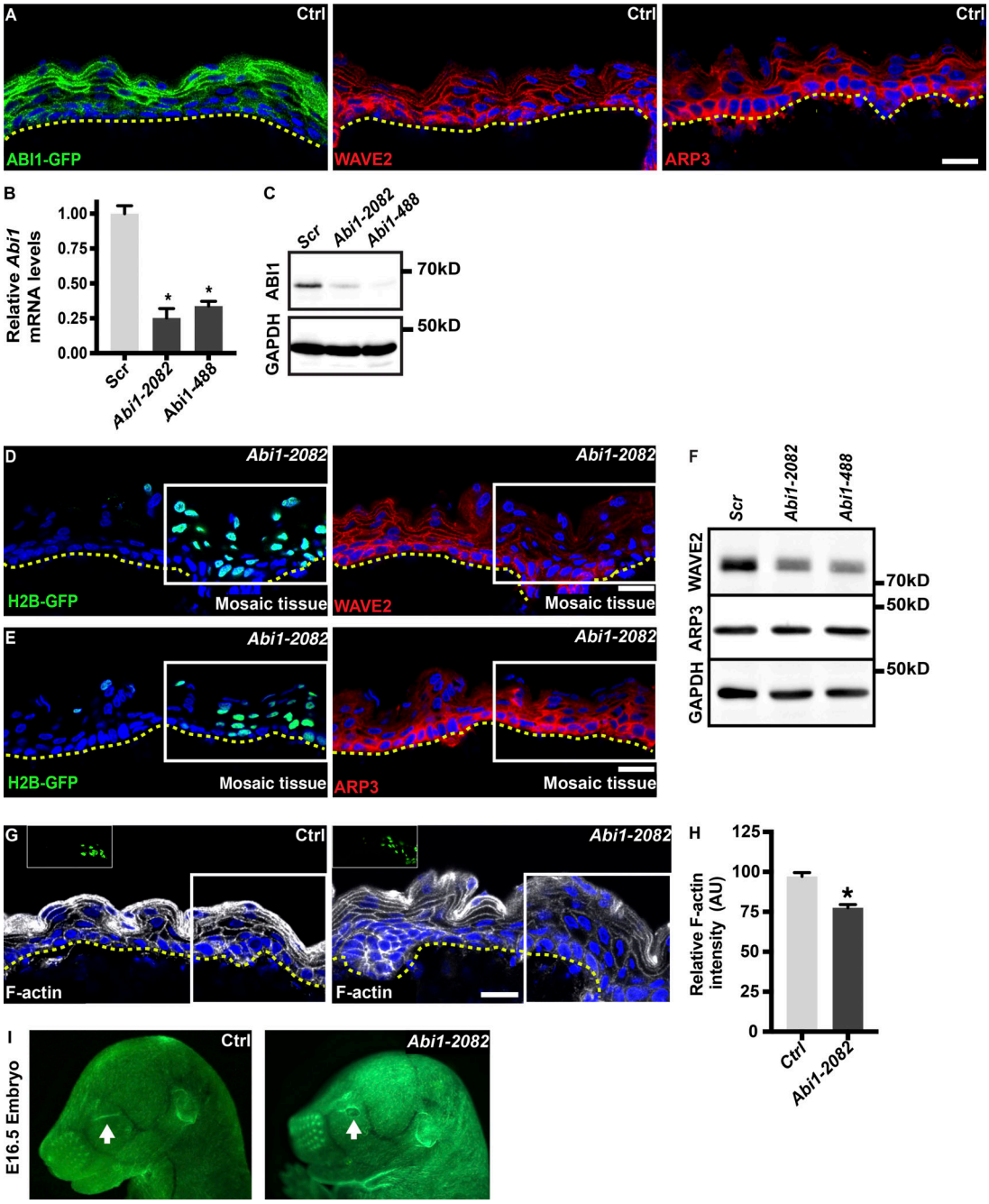

Figure 1. ***Abi1* depletion in the developing epidermis affects the actin cytoskeleton. (A)** Sagittal views of 10-µm sections of dorsal skin from E16.5 CD1 mouse embryos. Left: Embryos were injected on E9 with an *ABI1-GFP*-encoding lentivirus. Middle and right: Control embryos were immunostained for Wave2 (middle) or Arp3 (right). Nuclei were stained with DAPI (blue). Dotted lines indicate the dermal–epidermal border. Scale bars = 20 µm. **(B)** Quantitative PCR analysis of *Abi1* mRNA in primary mouse keratinocytes transduced with scrambled (*Scr*) shRNA or one of two *Abi1*-specific shRNAs (2082 and 488). Data are the mean ± SD of four preparations. *, P = 10^{-4} (*Scr* vs. *Abi1-2082*); *, P = 10^{-4} (*Scr* vs. *Abi1-488*) by unpaired *t* test. **(C)** Western blot analysis of primary mouse keratinocytes transduced with *Scr*, *Abi1-2082*, or *Abi1-488* shRNAs. Blots were probed with antibodies to ABI1 and GAPDH (loading control). **(D and E)** Sagittal views of 10-µm sections of dorsal skin from E16.5 CD1 embryos injected on E9 with an *Abi1-2082;H2B-GFP* lentivirus. Left panels show H2B-GFP fluorescence, and right panels show immunostaining for Wave2 (D) or Arp3 (E). White boxes indicate the location of transduced GFP⁺ cells in mosaic tissues. Nuclei were stained with DAPI. Dotted lines indicate the dermal–epidermal border. Scale bars = 20 µm. **(F)** Western blot analysis of primary mouse keratinocytes transduced with *Scr*, *Abi1-2082*, or *Abi1-488* shRNAs. Blots were probed with antibodies to Wave2, Arp3, and GAPDH (loading control). **(G)** Sagittal views of 10-µm sections of dorsal skin from E16.5 CD1 embryos injected on E9 with *shScr;H2B-GFP* (control, Ctrl) or *shAbi1-2082;H2B-GFP* lentiviruses. Sections were stained with fluorescent phalloidin (white) to visualize F-actin. White boxes and insets indicate the location of transduced GFP⁺ cells in the mosaic tissue. Dotted lines indicate the dermal–epidermal border. Nuclei were stained with DAPI (blue). Scale bar = 20 µm. **(H)** Quantification of F-actin staining intensity shown in G. Bars represent the mean phalloidin intensity ratio between infected (GFP⁺) and uninfected (GFP⁻) cells. Data are the mean ± SD from four control and four *shAbi1* KD embryos. *, P = 10^{-4} by unpaired *t* test. **(I)** Stereomicroscopic images of E16.5 embryos infected on E9 with *shScr;H2B-GFP* (Ctrl) or *shAbi1-2082;H2B-GFP* lentiviruses. Arrow indicates an open eye.

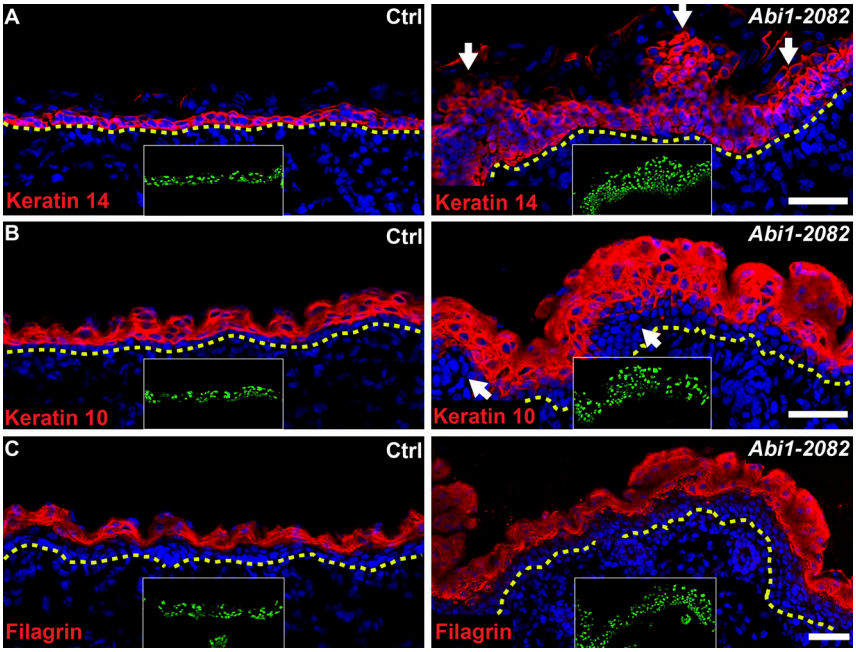

Figure 2. **Depletion of *Abi1* induces basal layer expansion and disruption of the epidermal architecture. (A–C)** Sagittal views of 10-µm sections of dorsal skin from control and *shAbi1-2082* KD E16.5 embryos. Sections were immunostained for the basal layer marker keratin 14 (A), the spinous layer and differentiation marker keratin 10 (B), and the granular layer marker filaggrin (C). Nuclei were stained with DAPI. Arrows indicate abnormal epidermal organization, dotted lines indicate the dermal–epidermal border, and insets show the transduced cells ($H2B^{-}GFP^{+}$). Scale bars = 50 µm.

Importantly, these defects were recapitulated in embryos transduced on E9 with a lentivirus carrying another *Abi1*-specific shRNA (*shAbi1-488*) and examined on E16.5 (Fig. S1). Moreover, overexpression of a shRNA-resistant cDNA encoding human ABI1-GFP in *Abi1* KD epidermis (*shAbi1-2082;ABI1-GFP*, rescue virus) restored a normal IFE phenotype, demonstrating the specificity of our KD approach (Fig. S1).

To determine if the hyperthickened epidermis and abnormal organization of the $K14^{+}$ basal layer cells result from HF evagination (Zhang et al., 2011), we labeled the back skins of E16.5 embryos for SOX2, a marker of all dermal papilla at E16.5 (Driskell et al., 2011). In both control and *Abi1* KD epidermis, $SOX2^{+}$ dermal papilla were detected next to the developing HFs in the dermis but not in the epidermis (Fig. S2).

Analysis of the distribution of the differentiation marker K10 in the back skin of wild-type and *Abi1*-depleted E13.5, E14.5, and E15.5 embryos showed comparable staining (Fig. S3). Moreover, when control and *Abi1* KD primary mouse keratinocytes were induced to differentiate in tissue culture, comparable levels of the differentiation markers K10 and loricrin were detected by Western blot analysis (Fig. S3). Collectively, these results demonstrate that ABI1 expression is essential for epidermal morphogenesis and organization of the basal layer but not for cell differentiation.

Abi1 depletion induces hyperproliferation of IFE cells

Our results thus far suggest that loss of *Abi1* induces abnormal tissue architecture and expansion of the epidermal basal layer, supporting a possible role for the Wave complex in controlling epidermal morphogenesis and cell proliferation. To investigate effects of *Abi1* KD on cell proliferation, we immunostained E16.5 dorsal skin for Ki67, a cell proliferation marker, and for phospho-histone H3 (pHH3), which specifically labels cells in mitosis. In control IFE, Ki67 staining was observed in most basal layer cells and only rarely in suprabasal cells (Fig. 3 A), and $pHH3^{+}$ cells were less abundant and were restricted to the basal layer (Fig. 3 B). In sharp contrast, *Abi1*-depleted epidermis showed abundant $Ki67^{+}$ cells in the two to three most basal cell layers and in aggregates of cells up to 15 layers in depth (Fig. 3 A). Similarly, $pHH3^{+}$ cells were more frequent in *Abi1* KD epidermis, particularly in the suprabasal layers (Fig. 3 B). To quantify these cell proliferation defects, we pulsed E16.5 pregnant mice for 2 h with BrdU, which incorporates into S-phase cells, and embryos were then removed for analysis of skin sections. Notably, the proportion of $BrdU^{+}$ cells was increased by ∼1.5-fold in the basal layer and by approximately threefold in suprabasal cells of *Abi1* KD compared with control embryos (42 ± 3% vs. 62 ± 1% and 4.8 ± 1% vs. 16.1 ± 2%, respectively; Fig. 3, C and D). As was observed for the morphological changes, these proliferation defects were recapitulated in embryos transduced with lentivirus carrying *shAbi1-488* (Fig. S1).

Abi1-depleted epidermis shows BM and spindle orientation defects

We next addressed whether epidermal loss of *Abi1* affects processes that regulate morphogenesis. We recently demonstrated that BM assembly and spindle orientation not only are regulated by the actin cytoskeleton but also play a major role in regulating IFE morphogenesis (Dor-On et al., 2017). To determine whether *Abi1* depletion affects BM organization, we examined control and *Abi1* KD dorsal skin sections at E16.5 for expression of the BM protein nidogen and the adhesion receptor integrin β4. As shown in Fig. 3 (E and F), both proteins are localized to the BM, which appears as a thin continuous line separating the epidermal and dermal layer. However, in *Abi1* KD embryos, the IFE showed large patches of diffuse staining of both nidogen and β4 integrin, often in highly convoluted patterns (Fig. 3, E and F).

To quantify spindle orientation, we examined the expression of survivin, which stains the cleavage furrow in late-mitotic cells, and then calculated the angle between the two daughter

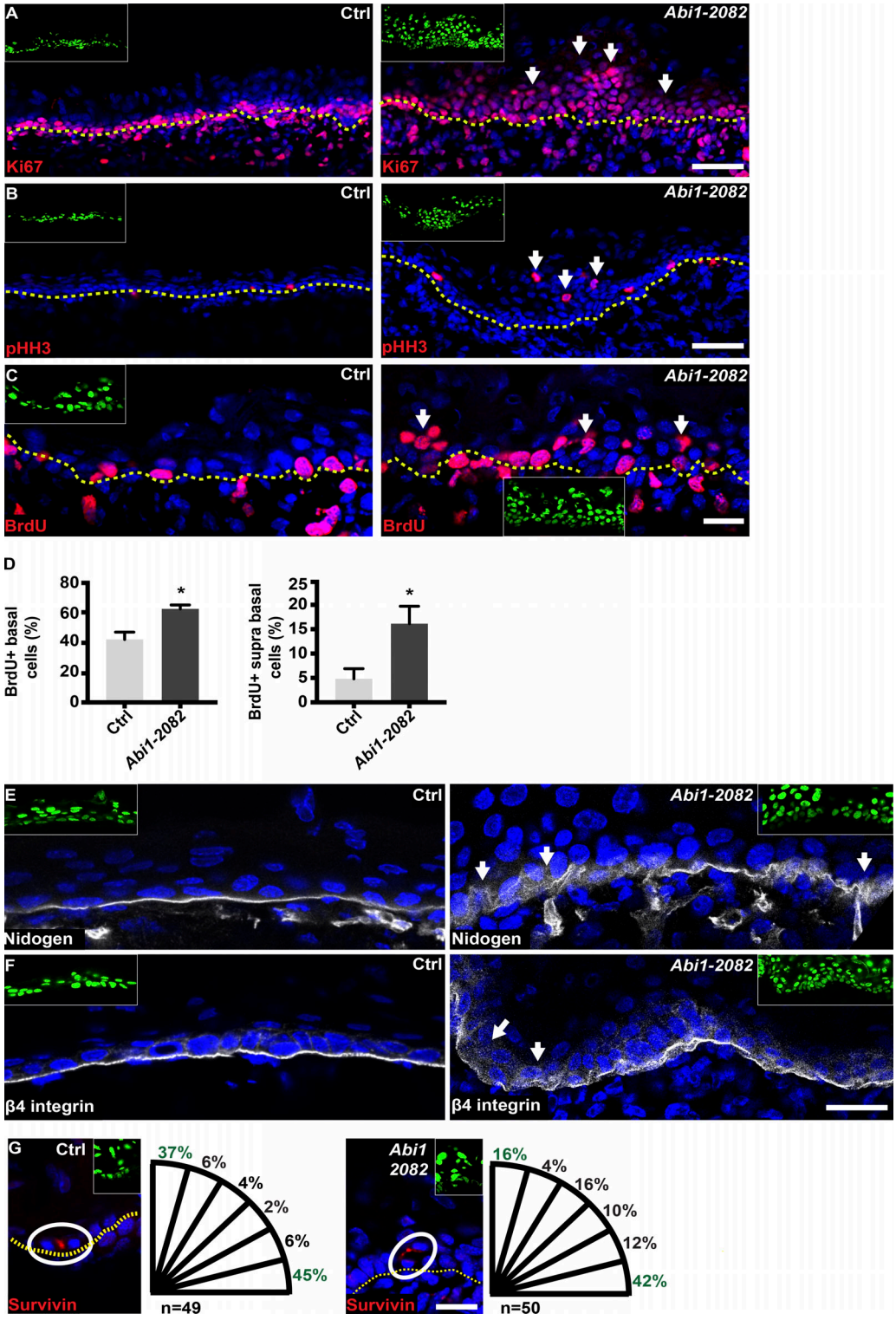

Figure 3. **Depletion of *Abi1* induces hyperproliferation and defects in BM organization and spindle orientation. (A and B)** Sagittal views of 10-µm sections of dorsal skin from control and *Abi1-2082* KD E16.5 embryos. Sections were immunostained for the cell proliferation markers Ki67 (A) and pHH3 (B). **(C)** Embryos were treated as described for A and B and pulsed for 2 h with BrdU on E16.5. In A–C, arrows indicate suprabasal mitotic cells. **(D)** Quantification of $BrdU^+$ cells in the basal and suprabasal sections of C. Data are the mean ± SD from four control and four *shAbi1* KD embryos. *, P = 0.0082 (basal cells); *, P = 0.015 (suprabasal cells) by unpaired *t* test. **(E and F)** Dorsal skin sections from embryos treated as in A and B. Sections were immunostained for nidogen (E) or β4 integrin (F). Arrows denote abnormal organization of BM. **(G)** Dorsal skin sections from embryos treated as in A and B and immunostained for the cleavage furrow marker survivin. White circles indicate survivin-positive, late-mitotic cells. Quantification of spindle orientation is presented to the right of each image. In A–C and G, dotted lines indicate the dermal–epidermal border. In A–C and E–G, insets show the transduced cells ($H2B^-GFP^+$). Nuclei were stained with DAPI (blue). Scale bars = 50 µm (A and B) and 20 µm (C and E–G).

nuclei and the BM (Williams et al., 2011; Dor-On et al., 2017). In control IFE, ∼40% of mitotic spindles were oriented perpendicular or parallel (75° to 90°) to the BM, and <20% of cell divisions were oblique (15° to 75°). However, *Abi1* KD caused a marked change in spindle orientation, with a >50% reduction in perpendicular spindle orientations and a 100% increase in oblique divisions (15° to 75°; Fig. 3 G). Together, these results suggest that loss of ABI1 markedly perturbs key processes that regulate tissue morphogenesis.

ABI1 loss of function does not alter the number of immune cells in the skin

Our results thus far suggest that loss of ABI1 induces defects in BM assembly and cell proliferation. Interestingly, β1 integrin KO mice also exhibit defects in both BM organization and cell proliferation (Raghavan et al., 2000; Hegde and Raghavan, 2013). Recently, Kurbet et al. (2016) identified a link between BM defects and recruitment of immune cells in the developing skin of β1 integrin KO mice. Therefore, we asked whether ABI1 loss-of-function phenotype involves changes in the number of immune cells into the skin. We immunostained E16.5 and E18.5 dorsal skin for CD45, an immune cell marker; however, a similar number of $CD45^+$ cells was detected in the skins of control and *Abi1* KD embryos (Fig. S2).

Wave2 loss of function phenocopies *Abi1* KD

In addition to being an essential component of the Wave complex, ABI1 also has Wave complex–independent functions, such as regulation of actin polymerization through nWASP (Innocenti et al., 2005) and the formin Diaphanous (Ryu et al., 2009), regulation of actin-capping activity (Innocenti et al., 2003), and regulation of Abl kinase activity (Shi et al., 1995). To determine if the *Abi1* KD phenotype in the developing mouse epidermis reflects loss of Wave complex–dependent or –independent ABI1 activity, we examined the effects of shRNA-mediated KD of *Wasf2*. We identified two shRNAs termed *Wasf2-493* and *Wasf2-269* that reduced *Wasf2* mRNA abundance in primary keratinocytes by 73 ± 0.5% and 65.4 ± 4.6%, respectively (Fig. S4), and CD1 embryos were injected on E9 with control shRNA or the identified *Wasf2-493* or *Wasf2-269*, as described for *Abi1* KD. Similar to the effects of *Abi1* KD, embryos injected with *shWasf2; H2B-GFP* on E9 had open eyes on E16.5 (Fig. S4). Moreover, dorsal skin from E16.5 *Wasf2* KD embryos showed morphological changes similar to those in *Abi1* KD epidermis; namely, expansion of $K14^+$ basal layer cells and readily detectable staining of the differentiation markers K10 and filaggrin (Fig. S4). Moreover, the proliferation defects observed in *Abi1* KD IFE were also recapitulated in *Wasf2*-depleted IFE (Fig. S4). These data confirm that the phenotype of *Abi1*-depleted IFE is due to perturbation of its function in the Wave complex.

Abi1-depleted epidermis shows a defect in HF development

We next analyzed whether *Abi1* loss of function affected the development of HFs. In the dorsal skin, HF development starts at approximately E14 and ends postnatally (Paus et al., 1999). Three morphologically distinguishable stages of HF formation are detectable by E16.5: basal cell thickening and elongation and formation of placodes, keratinocyte proliferation and downgrowth and formation of hair germs, and—the most advanced stage—keratinocyte formation of concave basal border and formation of hair pegs (Paus et al., 1999). The actin cytoskeleton is known to play a role in placode formation (Ahtiainen et al., 2014), whereas Arp2/3 loss of function decreases the number of HFs (Zhou et al., 2013). To determine if ABI1 activity affects the abundance of dorsal HFs, we immunostained E16.5 skin sections for P-cadherin, which is highly expressed in HFs (Rhee et al., 2006), and imaged the epidermis in planar view. Notably, control and *Abi1* KD epidermis showed no significant difference in the number of HFs (∼50 HFs per field of view; Fig. 4, A and B).

To determine if ABI1 activity affects HF morphogenesis, we quantified the number of placodes, germs, and pegs in dorsal skins. In control epidermis, ∼45%, ∼35%, and ∼20% of the HFs were at the placode, germ, and peg stages, respectively (Fig. 4, A and C). In contrast, *Abi1* KD epidermis showed a significant decrease in the number of germs and pegs (∼35% and ∼50% reductions, respectively) but not the number of placodes (Fig. 4, A and C). Together, these results suggest that although loss of ABI1 is not essential for HF abundance, its KD perturbs HF morphogenesis.

Abnormal distribution of the HF transcription factors SOX9 in *Abi1*-depleted epidermis

To better understand the defects in HF growth induced by *Abi1* depletion, we focused on the transcription factors SOX9, that play key roles in HF growth (Vidal et al., 2005; Nowak et al., 2008; Ouspenskaia et al., 2016). SOX9 was detected only in close proximity to the developing HFs in control E16.5 epidermis. In placodes, SOX9 was detected in suprabasal cells above the P-cadherin–rich HF cells, whereas at more advanced stages, SOX9 was present in P-cadherin–low cells of the developing HF that grow into the dermis (Fig. 4 D). Unexpectedly, in *Abi1*-depleted epidermis, SOX9 was also detected outside the developing HFs in IFE cells (Fig. 4, D and E). Moreover, SOX9 was detected in the nuclei of up to eight cell layers in foci of abnormally thick epidermis (Fig. 4 F). Quantification of $SOX9^+$ cells in sagittal sections that were colabeled for SOX9 and P-cadherin revealed that loss of ABI1 increased the expression of SOX9 in the IFE from ∼10% to ∼40% of basal layer cells ($SOX9^+$ and P-cadherin–low cells; Fig. 4, E and G). Similarly, whole-mount immunofluorescence microscopy also revealed ectopic expression of SOX9 in the IFE of *Abi1* KD epidermis (Fig. 4 H). Importantly, this finding was recapitulated in embryos transduced with lentiviruses carrying *shAbi1-488* (Fig. S1) or *shWasf2-493* (Figs. 4 G and S4), indicating that the aberrant up-regulation of SOX9 was due to the disruption of normal Wave complex-mediated functions. Collectively, these results suggest that Wave complex activity is essential for normal distribution of $SOX9^+$ cells in the IFE.

Overexpression of *Sox9* in the epidermis induces defects in cell proliferation, BM organization, and spindle orientation

In basal cell carcinoma, ectopic SOX9 activity has been shown to regulate cell stemness, BM organization, and spindle orientation (Larsimont et al., 2015), all of which are dependent on *Abi1/Wasf2*

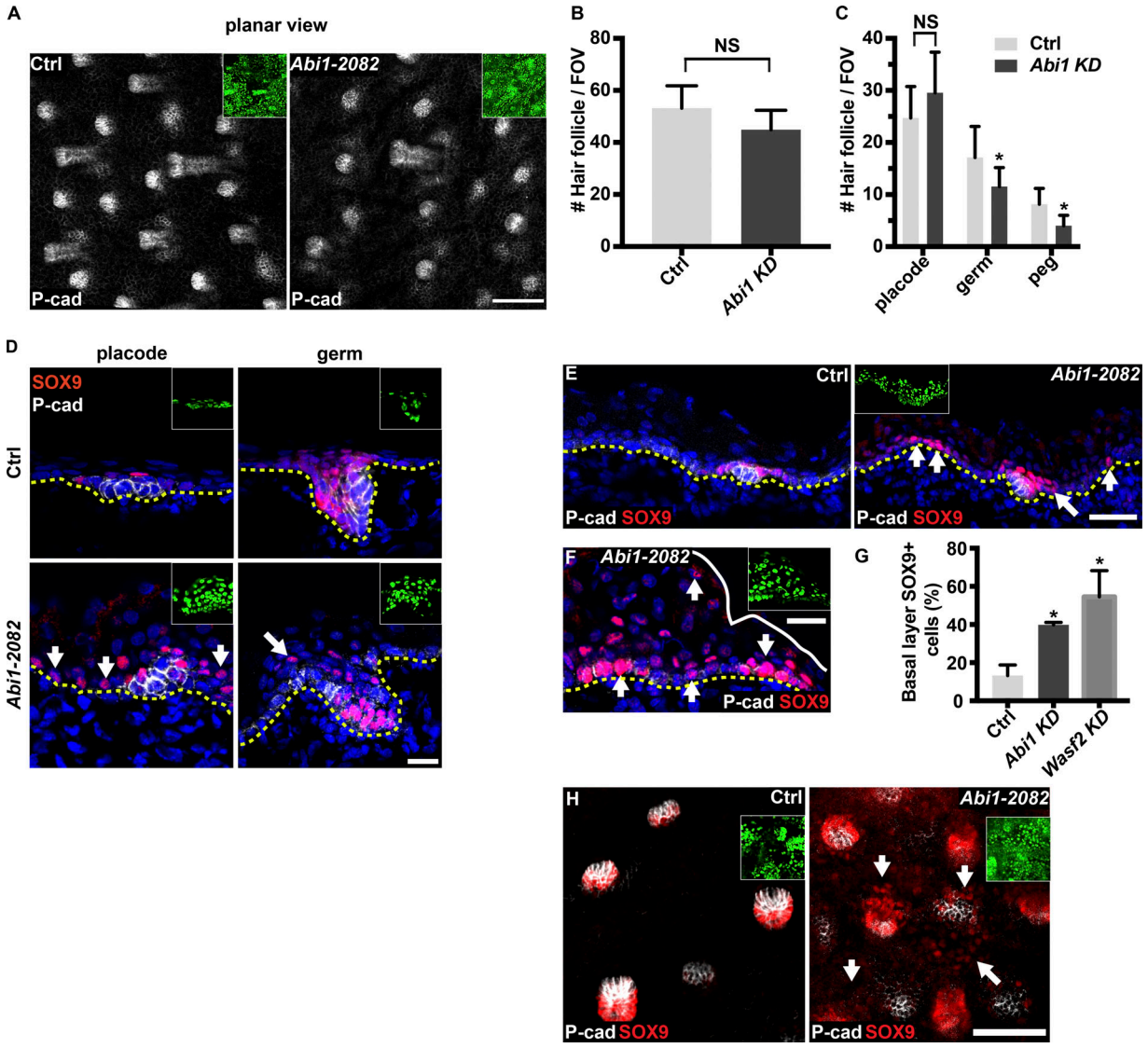

Figure 4. **Depletion of *Abi1* affects hair follicle development and distribution of the hair-follicle transcription factor SOX9. (A)** Whole-mount immunofluorescence of control and *Abi1-2082* KD E16.5 embryo immunostained for the hair follicle marker P-cadherin. **(B and C)** Quantification of data shown in A. Data are the means ± SD from four embryos per condition. *, $P = 5 \times 10^{-3}$ (germs); *, $P = 7 \times 10^{-5}$ (pegs) for control versus *Abi1-2082* KD cells by unpaired *t* test. **(D–F)** Sagittal views of 10-µm sections of dorsal skin from control and *Abi1-2082* KD E16.5 embryos. Sections were immunostained for P-cadherin and SOX9. Arrows indicate abnormal distribution of SOX9. **(G)** Quantification of basal layer SOX9 staining shown in E and in sections from embryos injected in the same manner with *shWasf2-493;H2B-GFP* lentivirus. Data are the mean ± SD from four control, four *Abi1,* and three *Wasf2* embryos. *, P = 0.0017 (Ctrl vs. *Abi1-2082*); *, P = 0.024 (Ctrl vs. *Wasf2-493*) by unpaired *t* test. **(H)** Whole-mount immunofluorescence of control and *Abi1-2082* KD E16.5 embryos immunostained for SOX9. In the images, insets show the transduced cells ($H2B^{-}GFP^{+}$), and dotted lines indicate the dermal–epidermal border. Nuclei were stained with DAPI (blue). Scale bars = 100 µm (A), 20 µm (D and F), and 50 µm (E and H). FOV, field of view.

in the developing IFE. Moreover, overexpression in cultured human keratinocytes and adult rat epidermis increases cell proliferation and negatively affects differentiation (Shi et al., 2013).

These reports, and the fact that SOX9 function in IFE development remains unclear, prompted us to investigate the possibility that the observed functions of the Wave complex in the developing IFE might be mediated, at least in part, through ectopic expression of SOX9.

To determine whether forced SOX9 overexpression in the developing epidermis could recapitulate the phenotype of Wave complex loss-of-function embryos, we injected embryos with *GFP* (control) or *Sox9* expressing lentiviruses (Guo et al., 2012) on E9 and analyzed dorsal skin sections at E16.5. *Sox9-tg* epidermis showed an abnormal pattern of SOX9 expression, with most IFE cells staining positive (Fig. 5 A). To examine cell proliferation, the BrdU analogue 5′ethynyl-2-deoxyuridine (EdU) was injected into E16.5 pregnant mice, and the embryos were removed and the dorsal skin sections analyzed 2 h later. We found that *Sox9-tg* epidermis contained ∼35% more EdU^{+} basal layer cells that did control epidermis (38 ± 1.5% vs. 52 ± 3%, respectively) and ∼600% more EdU^{+} suprabasal layer cells (2 ± 0.5% vs. 12 ± 1.5%, respectively; Fig. 5, B and C).

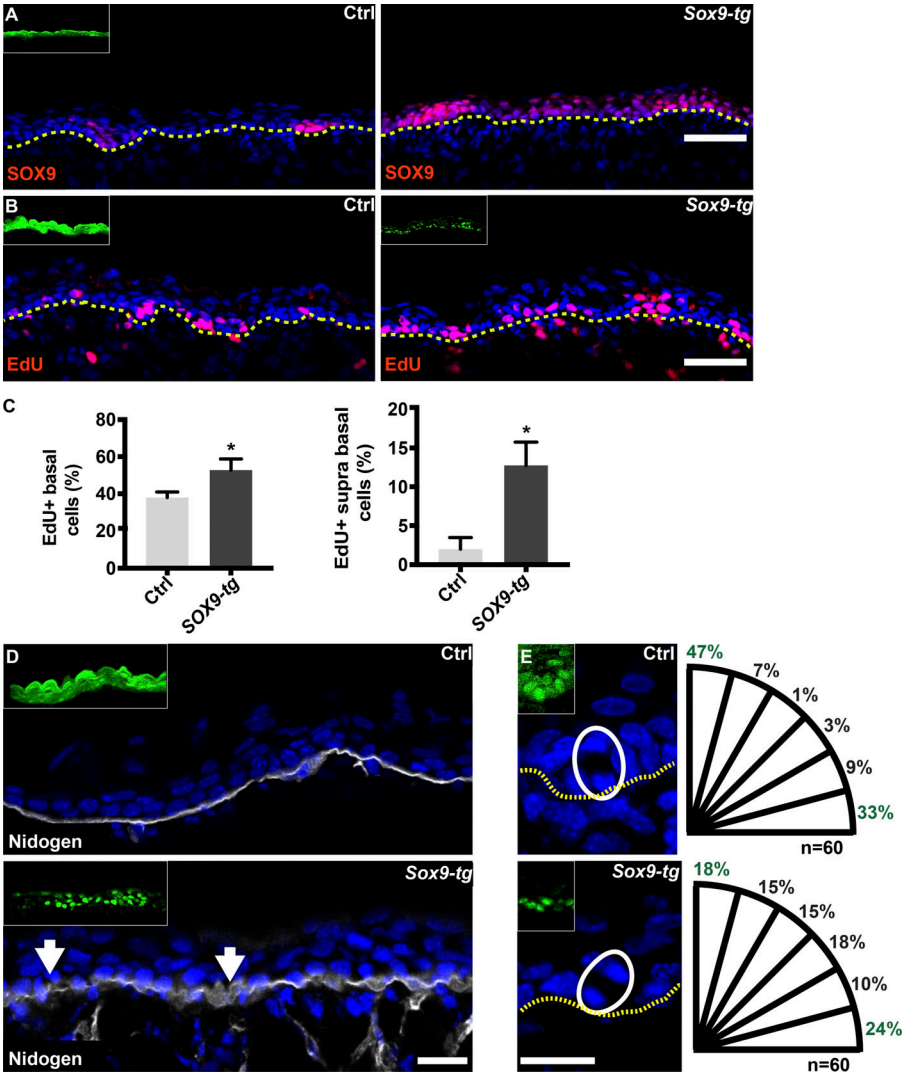

Figure 5. **SOX9 overexpression induces hyperproliferation and defects in BM organization and spindle orientation. (A and B)** Sagittal views of dorsal skin from control and embryos injected on E9 with *Sox9*-expressing lentivirus. Sections were immunostained for SOX9. **(B)** Embryos treated as described for A were pulsed for 2 h with EdU on E16.5 and then imaged. Inset shows transduced cells (GFP for control and immunostained for SOX9). **(C)** Quantification of EdU$^+$ cells in the basal and suprabasal layers in B. Data are the mean ± SD from four embryos per condition. *, P = 0.01 (basal cells); *, P = 0.02 (suprabasal cells) by unpaired *t* test. **(D)** Sections of dorsal skin from E16.5 embryos treated as in A and B were immunostained for nidogen. Arrows indicate diffuse staining. Inset shows transduced cells (GFP for control and immunostained for SOX9). **(E)** Sections of dorsal skin from E16.5 embryos treated as in A and B. White circles indicate late-mitotic cells, and dotted lines indicate the dermal–epidermal border. Quantification of spindle orientation is presented to the right of each image. Inset shows transduced cells (GFP for control and immunostained for SOX9). Scale bars = 50 µm (A and B) and 20 µm (D and E).

We also examined the effects of forced SOX9 expression on BM organization and spindle orientation. Similar to the effects of *Abi1* KD, the epidermis of E16.5 *Sox9-tg* embryos displayed large patches of diffuse nidogen staining in an irregular pattern (Fig. 5 D). Similarly, calculation of the angle between the BM and two daughter nuclei of late-mitotic cells (Luxenburg et al., 2011) revealed an ∼250% reduction in perpendicular spindle orientation (75° to 90°) and an ∼300% increase in oblique divisions (15° to 75°) in the basal cells of *Sox9-tg* embryos compared with control embryos (Fig. 5 E), which was comparable to the effects of *Abi1* KD.

These results therefore suggest that enhanced SOX9 expression recapitulates the tissue morphogenesis and cell proliferation defects observed in the developing mouse IFE of *Abi1/Wasf2* KD embryos.

Abi1/Wasf2-depleted epidermis shows abnormal Wnt signaling

Next, we asked how loss of Wave complex activity can induce SOX9 expression in the developing IFE. Recently, Ouspenskaia et al. (2016) used lentivirus-mediated manipulation of genes that regulate Wnt signaling to show that SOX9$^+$ cell specification is controlled by the juxtaposition of Wnt^{hi} and Wnt^{lo} cells in mosaic tissue. This finding raised the possibility that the aberrant expression of SOX9 in *Abi1/Wasf2* KD IFE might result from perturbation of normal Wnt signaling.

When the canonical Wnt signaling pathway is active, the adherens junction (AJ) protein β-catenin becomes stabilized and functions as a nuclear cofactor (Lim and Nusse, 2013; Veltri et al., 2018). We therefore asked whether *Abi1* KD affects Wnt signaling by examining the localization and phosphorylation status of β-catenin.

In control embryos, we found that nuclear β-catenin was detected only at the developing HFs (Fig. 6 A). In *Abi1* KD epidermis, nuclear β-catenin was also detected in the nuclei of basal and suprabasal layer cells of the IFE (Fig. 6 A). To verify these observations, we used an antibody that specifically detects the nonphosphorylated form of β-catenin (Amit et al., 2002). Consistent with our previous results, control IFE showed strong nonphosphorylated β-catenin expression in the basal layer and lower expression in the suprabasal layers (Fig. 6 B). In sharp contrast, nonphosphorylated β catenin was highly expressed in the suprabasal layers of *Abi1* KD IFE (Fig. 6 B), and quantification

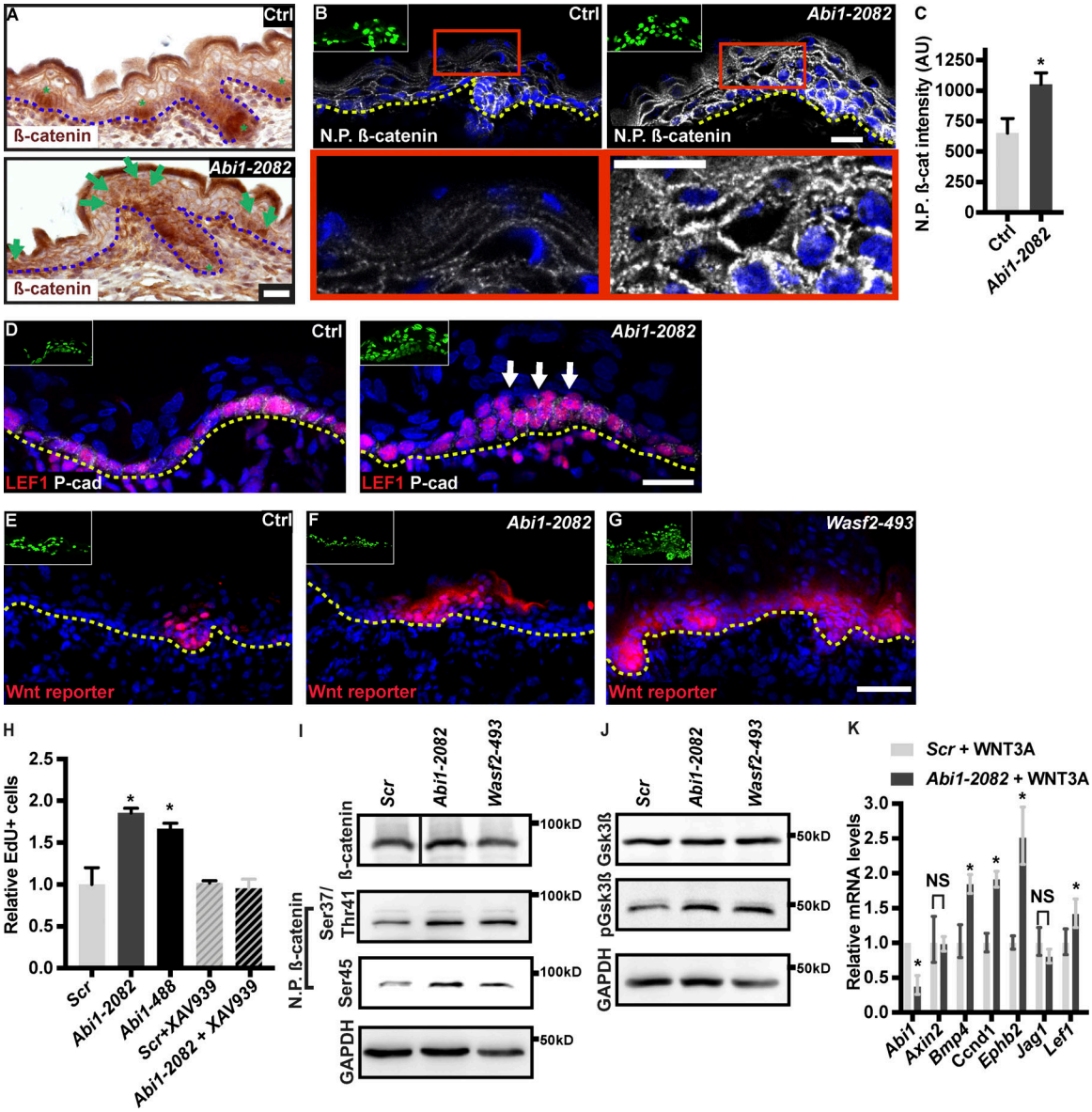

Figure 6. ***Abi1*-depleted epidermis exhibits defects in β-catenin localization and Wnt signaling. (A and B)** Sagittal views of 10-µm dorsal skin sections from control and *Abi1-2082* KD E16.5 dorsal skin immunostained for β-catenin (A) or nonphosphorylated (N.P. Ser45) β-catenin (B). Lower panels show digital magnifications (3×) of the red boxes in the upper panels. Insets show transduced cells (GFP⁺). Green asterisks in A indicate developing HFs. Green arrows in A indicate nuclear β-catenin in the IFE. **(C)** Quantification of nonphosphorylated β-catenin intensity from the images shown in B. Data are the mean ± SD of four embryos per condition. *, P = 0.0023 by unpaired *t* test. **(D)** Sagittal views of 10-µm dorsal skin sections from control and *Abi1-2082* KD E16.5 dorsal skin coimmunostained for LEF1 and P-cadherin. Arrows denote suprabasal LEF1. **(E–G)** Sagittal views of 10-µm sections of dorsal skin from E16.5 CD1 embryos injected on E9 with lentiviruses expressing *Wnt reporter-RFP* plus *shScr;H2B-GFP* (E), *Wnt reporter-RFP* plus *shAbi1-2082;H2B-GFP* (F), and *Wnt reporter-RFP* plus *shWasf2-493;H2B-GFP* (G). **(H)** Primary mouse keratinocytes were transduced with *shScr*, *shAbi1-2082*, or *shAbi1-488* shRNAs. Cells were left untreated or treated with 5 µM XAV939 for 24 h, pulsed for 3 h with EdU, and analyzed. Data are the mean ± SD of four experiments. *, P = 0.002 (Ctrl vs. *Abi1-2082*); *, P = 0.004 (Ctrl vs. *Abi1-488*), by unpaired *t* test. **(I)** Western blot analysis of primary mouse keratinocytes transduced with *Scr*, *Abi1-2082*, or *Wasf2-493* shRNAs. Blots were probed with antibodies to β-catenin, nonphosphorylated (Ser45) β-catenin, nonphosphorylated (Ser37/Thr41) β-catenin, and GAPDH (loading control). **(J)** Western blot analysis of primary mouse keratinocytes transduced with *Scr*, *Abi1-2082*, or *Wasf2-493* shRNAs. Blots were probed with antibodies to GSK3β, phosphorylated GSK3β, and GAPDH (loading control). **(K)** Quantitative PCR analysis of Wnt target genes in primary mouse keratinocytes transduced with *shScr* or *shAbi1-2082* shRNAs and treated with 10 ng Wnt3a for 12 h. Data are the mean ± SD of four preparations. *, P < 0.05. Insets in B and D–G show transduced cells (H2B⁻GFP⁺). N.P. β-catenin indicates nonphosphorylated β-catenin. Dotted lines indicate the dermal–epidermal border. Nuclei were stained with DAPI (blue). Scale bars = 20 µm (A, B, and D) and 50 µm (G).

of staining intensity revealed a significant, approximately two-fold increase in nonphosphorylated β-catenin intensity in suprabasal cells of the *Abi1* KD epidermis (Fig. 6 C). Moreover, in the developing epidermis, WNT^{hi} cells are positive for the transcription factor LEF1 (Ouspenskaia et al., 2016). In control epidermis, LEF1⁺ cells were restricted to the basal layer; however, LEF1⁺ cells were detected also in suprabasal layers in the *Abi1*-depleted epidermis (Fig. 6 D).

To determine whether the increase in nonphosphorylated and nuclear-localized β-catenin levels observed in *Abi1*-depleted epidermis affects Wnt signaling, we injected E9 embryos with lentiviruses expressing *shScr* or *shAbi1* together with an RFP-tagged Wnt activity reporter (Beronja et al., 2013). Examination of dorsal skin sections on E16.5 showed that Wnt reporter activity was restricted to the developing HFs in control epidermis (Fig. 6 E), which is consistent with previous reports (DasGupta and Fuchs, 1999; Beronja et al., 2013; Rognoni et al., 2014). In contrast, in *Abi1*-depleted epidermis and *Wasf2*-depleted epidermis, Wnt activity was detected in both the HF and IFE (Fig. 6, F and G; and Fig. S4).

Work in the developing epidermis (Ouspenskaia et al., 2016) and in cultured keratinocytes (Ghahramani et al., 2018) demonstrated the strong non–cell autonomous effects of Wnt signaling on SOX9 expression (Ouspenskaia et al., 2016) and cell proliferation (Ghahramani et al., 2018). In line with that, immunofluorescence analysis of mosaic *Abi1* KD tissue showed ectopic expression of SOX9, the proliferation marker Ki67, and expansion of the basal layer marker K14 in noninfected cells (wild type, GFP^-) that were adjacent to *Abi1* KD cells (GFP^+; Fig. S5). Taken together, these results suggest that Wave complex activity regulates β-catenin activation and localization and Wnt signaling in the developing epidermis.

Abi1 loss-of-function defects can be recapitulated in cultured keratinocytes

To determine if *Abi1* loss-of-function hyperproliferation phenotype can be recapitulated in cultured keratinocytes, we infected primary mouse keratinocytes with *shScr* (control), *shAbi1-2082*, or *shAbi1-488* viruses. 5 d after infection, cells were treated with EdU, and its incorporation was analyzed. Notably, the proportion of EdU^+ cells was increased by 85% in cells that were transduced with *shAbi1-2082* and 66% in cells that were transduced with *shAbi1-488* compared with control embryos (18 ± 1.8% vs. 33.4 ± 1% and 29.9 ± 1.2%; Fig. 6 H).

Wnt signaling is a positive regulator of keratinocyte proliferation in vivo (Choi et al., 2013; Lim et al., 2013) and in vitro (Ghahramani et al., 2018). To determine if the *Abi1* KD hyperproliferation is mediated by Wnt signaling, cells were transduced with *shScr* or *shAbi1-2082* viruses and treated with XAV-939, which antagonizes Wnt signaling (Beronja et al., 2013). Strikingly, XAV-939 treatment blocked the *Abi1* KD cell hyperproliferation (Fig. 6 H).

In line with the notion that Wnt signaling is up-regulated in Wave complex loss-of-function keratinocytes, Western blot analysis demonstrated an increase in nonphosphorylated β-catenin and an increase in GSK3β phosphorylation in both *Abi1*- and *Wasf2*-depleted cultured keratinocytes (Fig. 6, I and J). Moreover, when control and *Abi1* KD cells were treated with the Wnt ligand Wnt3a (10 nM) for 12 h, *Abi1* KD cells exhibited a significant up-regulation in the mRNA levels of canonical Wnt signaling target genes including Bmp4 (1.8-fold), Ccnd1 (1.9-fold), Ephb2 (2.5-fold), and Lef1 (1.4-fold; Fig. 6 K). Taken together, these results suggest that Wave complex affects canonical Wnt signaling and cell proliferation in cultured mouse keratinocytes.

Normal actin levels are essential for Wnt signaling homeostasis

Several actin-binding proteins were shown to regulate canonical Wnt signaling. For instance, the actin-nucleating protein formin 2 regulates canonical Wnt signaling in neural progenitor cells by mediating the transportation and endocytosis of Wnt components (Lian et al., 2016). Cancer-related regulator of actin dynamics (CARD) regulates Wnt signaling by increasing actin polymerization and stabilizing AJs in the intestinal epithelium (Jung et al., 2018). Because we found that *Abi1* depletion in the epidermis decreases F-actin content (Fig. 1) and concomitantly increases Wnt signaling (Fig. 6), we asked whether pharmacological manipulation of F-actin content can alter β-catenin localization in cultured keratinocytes. We treated cells with DMSO (control), 125 nM latrunculin, or 250 nM jasplakinolide (drugs that decrease [Morton et al., 2000] or increase [Bubb et al., 1994] F-actin content, respectively) for 30 min, and fixed and labeled the cells for β-catenin and nonphosphorylated β-catenin (Fig. 7 A). Analysis of nuclear β-catenin fluorescence intensity demonstrated that latrunculin treatment increased β-catenin fluorescence intensity of both total and nonphosphorylated β-catenin by ∼50% (48.6 ± 23.7% and 45.9 ± 10.2%, respectively), while jasplakinolide treatment did not alter nuclear staining intensity (Fig. 7, A and B).

Next, we asked whether enforced reduction of actin levels can induce ectopic Wnt signaling activity in the developing IFE. To analyze this, we injected E9 embryos with lentiviruses expressing *shScr* or β-actin–targeting shRNA (*shActb-289*) together with the Wnt activity reporter. We previously demonstrated that this shRNA reduces *Actb* mRNA abundance in keratinocytes by ∼50% (Dor-On et al., 2017). Similar to the effects of *shAbi1* transduction, *Actb* depletion induced ectopic Wnt reporter activity (Fig. 7 C), confirming that the actin cytoskeleton plays a vital role in maintaining normal Wnt activity in the developing epidermis.

ABI1 is not essential for cell–cell junction formation

Previous work has demonstrated an important role for ABI1 (Ryu et al., 2009; Xiong et al., 2012) and the Wave complex (Lee et al., 2016; Sasidharan et al., 2018) in AJ homeostasis. The pattern of β-catenin immunostaining in *Abi1* KD IFE had suggested that AJ formation was unaffected by the loss of Wave complex function (Fig. 6). To verify this result, we examined the localization of two additional AJ proteins, E-cadherin and α-catenin. Notably, both of these proteins were normally distributed at the periphery of IFE cells in dorsal skin sections of both control and *Abi1* KD E16.5 embryos (Fig. S6). Moreover, markers of desmosomes (desmoplakin) and tight junctions (occludin and ZO-1), which are essential cell–cell adhesion structures in the epidermis (Simpson et al., 2011), were also normally distributed in IFE sections from *Abi1* KD embryos (Fig. S6). Thus, Wave complex activity is not essential for the maintenance of cell–cell adhesion in the developing mouse epidermis.

Collectively, the results presented here demonstrate an essential role for the Wave complex in establishing the normal structure and function of the developing epidermis.

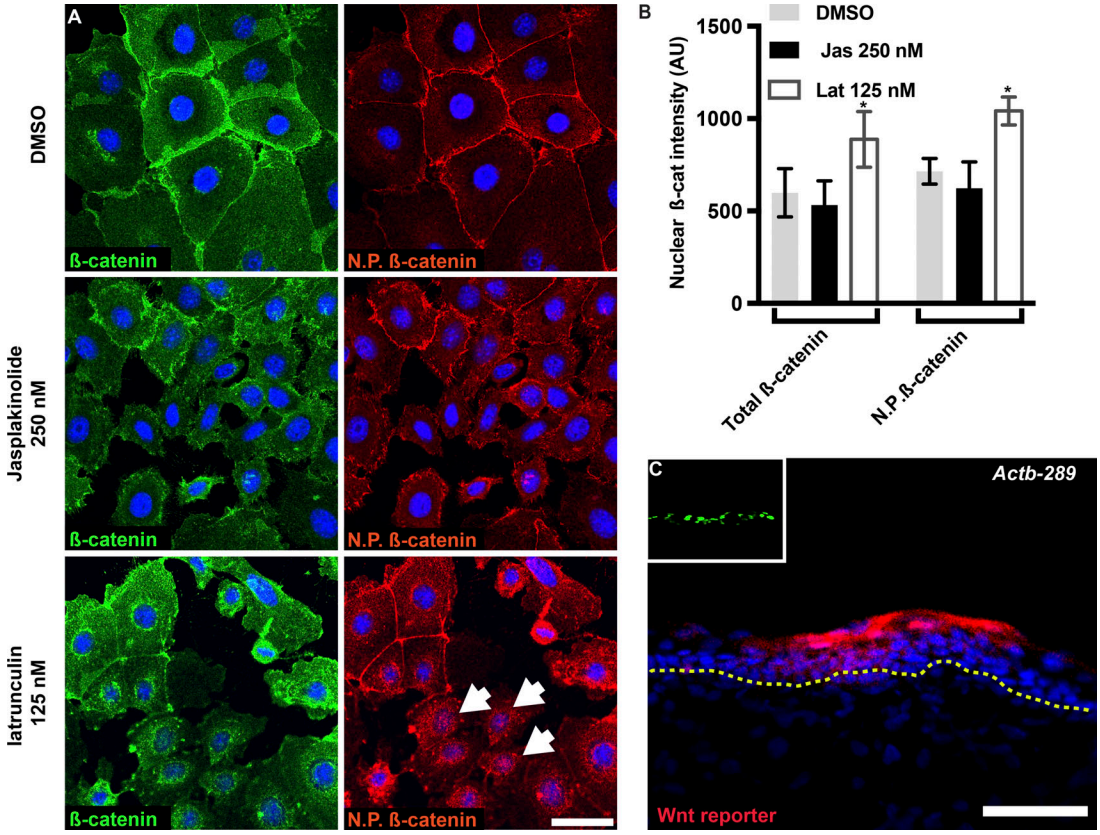

Figure 7. **The actin cytoskeleton regulates β-catenin localization and Wnt signaling. (A)** Wild-type keratinocytes were treated with DMSO (control), 250 nM jasplakinolide, or 125 nM latrunculin for 30 min, fixed, and labeled for β-catenin or nonphosphorylated (Ser45) β-catenin. **(B)** Quantification of β-catenin and nonphosphorylated (Ser45) β-catenin nuclear fluorescence intensity from the images shown in A. Data are the mean ± SD of 2,200 cells from three independent experiments. *, P = 0.013 for total β-catenin; *, P = 0.0073 for nonphosphorylated β-catenin, by unpaired *t* test. **(C)** Sagittal views of 10-µm sections of dorsal skin from E16.5 CD1 embryos injected on E9 with lentiviruses expressing *Wnt reporter-RFP* plus *shActb-289;H2B-GFP*. Nuclei were stained with DAPI (blue). Scale bars = 20 µm (A) and 50 µm (B).

Moreover, enhanced SOX9 expression recapitulates the tissue morphogenesis and cell proliferation defects observed in of *Abi1/Wasf2* KD embryos. Thus, we have uncovered a novel Wave complex–F-actin–Wnt/β-catenin–SOX9 pathway that regulates IFE development.

Discussion

In the last several decades, an impressive body of work has identified several signaling pathways that govern epidermal development and homeostasis. Defects in the fine tuning of these pathways can be detected in common skin diseases such as psoriasis and cancer (Fuchs, 2007; Blanpain and Fuchs, 2009; Roberts and Horsley, 2014; Rubsam et al., 2018). Our study has identified a novel role for the Wave complex in regulating one of these major pathways; namely, Wnt signaling. We showed that Wave complex activity regulates F-actin content and that proper actin levels are essential to control Wnt signaling and SOX9 expression and to maintain normal structure and function in the developing mouse epidermis. The physiological importance of this function is reflected in the striking defects in tissue shape and growth that occur when Wave complex activity is compromised.

Our results demonstrate that the loss of Wave complex activity and the loss of Arp2/3 complex activity give rise to distinct phenotypes in the developing epidermis (Zhou et al., 2013). While Arp2/3 activity is essential for epidermal differentiation, tight junction formation, and HF abundance, Wave complex activity is not essential for these processes/structures (Zhou et al., 2013). nWASP is another key NPF in the epidermis; however, its function was not explored during epidermal development. In the adult, it was shown to regulate IFE differentiation and tight junction formation (Kalailingam et al., 2017), and its loss resulted in hyperproliferation in the IFE (Lyubimova et al., 2010; Kalailingam et al., 2017) due to inflammation (Kalailingam et al., 2017). These results are in line with the notion that NPFs function downstream of different signaling cascades and differentially regulate Arp2/3-mediated actin polymerization, which plays a role in many biological processes. The need to tightly control actin polymerization is highlighted by the broad range of developmental defects in individuals that suffer from Baraitser–Winter syndrome, in which F-actin content is abnormal (Riviere et al., 2012).

In the epidermis, the small GTPase CDC42 (Wu et al., 2006) and its binding partner the NPF nWASP (Lyubimova et al., 2010) are positive regulators of Wnt signaling. While CDC42 is an

important regulator of the actin cytoskeleton, its ability to regulate Wnt signaling is completely dependent on PKCζ, which affects β-catenin degradation through the inhibition of GSK3β (Wu et al., 2006). Moreover, while the mechanism by which nWASP executes its regulatory function is not completely understood, it is interesting to note that actin-based processes such as wound healing are not affected by nWASP loss of function (Lyubimova et al., 2010). Unlike CDC42 or nWASP, our results demonstrate that the Wave complex suppresses Wnt signaling and that it is essential for key actin-based processes in the developing epidermis (i.e., eyelid closure, BM assembly, and spindle orientation).

Ectopic activation of Rho kinase (ROCK) increases Wnt signaling in the adult epidermis (Samuel et al., 2011). However, ROCK functions in many processes that do not involve actin polymerization, such as myosin II activity, microtubule stability, proliferation, and apoptosis (Amin et al., 2013; Wei et al., 2016). Our demonstration that moderate depletion of actin can trigger ectopic Wnt signaling highlights the critical role of the actin cytoskeleton in this signaling pathway, which is particularly interesting since abnormal actin levels are a feature of many cancers (Guo et al., 2013; Jung et al., 2018). Given the profound complexity of both the actin cytoskeleton and Wnt signaling, further work will be needed to fully understand the interaction between these two processes.

Wnt signaling has previously been implicated in controlling SOX9 expression in the developing epidermis (Ouspenskaia et al., 2016) and in basal cell carcinoma (Larsimont et al., 2015). This crucial transcription factor plays an essential role in HF development and homeostasis (Vidal et al., 2005; Nowak et al., 2008; Kadaja et al., 2014), and its aberrant expression contributes to neoplastic transformation of the epidermis (Vidal et al., 2005; Larsimont et al., 2015). In basal cell carcinoma, abnormal SOX9 expression leads to dysregulation of the actin cytoskeleton, disruption of epidermal differentiation, and remodeling of the BM (Larsimont et al., 2015). Our study adds novel insights into the function of SOX9 in the skin by identifying a previously unknown function for this transcription factor during embryonic development. We demonstrate that forced *Sox9* expression mimics the loss-of-function phenotype induced by *Abi1/Wasf2* KD in affecting BM assembly, spindle orientation, and cell proliferation. Interestingly, SOX9 transcriptional activity regulates the expression of actin genes in basal cell carcinoma (Larsimont et al., 2015). Since our study indicates that the actin cytoskeleton functions upstream of SOX9 in the epidermis, defects in the actin cytoskeleton could lead to ectopic SOX9 expression in pathological states.

ABI1 was first suggested to play a role in cancer more than 20 years ago, when Shi et al. (1995) showed that ABI1 overexpression suppresses the transforming activity of Abelson leukemia virus. Since then, ABI1 function has been explored in many cancer models in vitro and in vivo, and the results indicate that both loss and gain of *Abi1* function can affect cancer development and progression (Sun et al., 2009; Cui et al., 2010; Xiong et al., 2012; Steinestel et al., 2014). Although the current study focuses on epidermal development rather than cancer, the observed induction of ectopic Wnt signaling and *Sox9* expression induced by ABI1 loss of function are also observed in many types of cancers (Vidal et al., 2008). Thus, it will be of great interest to determine whether ABI1/Wave2 effects on Wnt signaling and SOX9 are also involved in the development and progression of cancer. Overall, our findings reveal a novel function for ABI1, Wave2, and the Wave complex in suppressing Wnt–SOX9 activity in a complex mammalian system in vivo.

Materials and methods

Mice and primary mouse keratinocytes

All experimental protocols were approved by the Tel Aviv University Animal Care and Use Committee. Hsd:ICR (CD1) mice (Harlan Biotech) were used for all experiments. Epidermal keratinocytes were isolated as previously described (Nowak and Fuchs, 2009). Briefly, dorsal skin was removed from newborn mice and incubated with dispase (Sigma-Aldrich), followed by isolation of the epidermis, which was treated with trypsin (Biological Industries). Keratinocytes were plated on fibroblast feeder cells for four passages and then plated in regular tissue culture dishes.

Lentivirus production

Lentiviruses were produced as previously described (Beronja et al., 2010; Luxenburg et al., 2015). Briefly, lentivirus plasmids were generated by oligonucleotide cloning into the following vectors: pLKO.1-TRC (gift from David Root, Broad Institute, Cambridge, MA; Addgene; 10878)], LV-GFP, or LV-RFP (both gifts from Elaine Fuchs, Rockefeller University, New York, NY; Addgene; 25999 and 26001, respectively) by digestion with EcoRI and AgeI, as described in the Genetic Perturbation Platform (GPP) website (http://portals.broadinstitute.org/gpp/public/resources/protocols). shRNA sequences were acquired from GPP (http://portals.broadinstitute.org/gpp/public/): *Abi1 (2082)* construct TRC350748, target sequence: 5′-TCCAATTTG TGTAACGATTAT-3′; *Abi1(488)* construct TRC321647, target sequence: 5′-GCTCGAAGAGAGATTGGTATT-3′; *Wasf2 (269)* construct TRC99314, target sequence: 5′-AGTAAGTATGCAGAG GACATT-3′; *Wasf2(493)* construct TRC99312, target sequence: 5′-GCCCGTCTTAGAGACCTATAA-3′; and *Actb(289)* construct: TRC90899, target sequence: 5′-CCATTGAACATGGCATTGTTA-3′.

The Abi1 rescue plasmid was generated by cloning human ABI1-GFP (pEGFP-Abi1, a gift from Giorgio Scita, University of Milan, Milan, Italy; Addgene; 74905; Innocenti et al., 2004) into the Abi1-2082-pLKO.1 plasmid digested with BamHI and KpnI. Abi1-2082 targets the 3′UTR of *Abi1* and therefore does not affect *ABI1* cDNA. The Sox9-expressing lentivirus plasmid was a gift from Robert Weinberg, Whitehead Institute, Cambridge, MA (pWPXL-Sox9, Addgene; 36979; Guo et al., 2012). The GFP-expressing lentivirus plasmid pWPXLd was used as a control and was a gift from Didier Trono, École polytechnique fédérale de Lausanne, Lausanne, Switzerland (Addgene; 12258). The Wnt reporter lentivirus was a gift from Elaine Fuchs (Beronja et al., 2013). Vesicular stomatitis virus G glycoprotein pseudotyped lentivirus was produced by transfection of 293FT cells (Invitrogen; R70007) followed by cell culture for 48–72 h. Viral

supernatant was collected, filtered through a 0.45-µm filter, and concentrated by ultracentrifugation using an Avanti JXN30 (Beckman Coulter). Viral titers were determined by FACS analysis of infected HeLa cells.

In utero lentivirus injection and controls

Lentiviruses were injected into gestating mice as previously described (Beronja et al., 2010). Briefly, females at E9 were anesthetized with isoflurane, and each embryo (up to six per litter) was injected with 0.1–1 µl of ∼2 × 10^9 colony-forming units of the appropriate lentiviruses. In the in vivo KD experiment, the term "control" was used when two sets of data were collected: (a) uninjected littermate embryos and (b) *shScr;H2B-GFP* lentivirus-injected embryos. For the *Sox9* overexpression experiment, "control" represents uninjected littermate embryos and *GFP* lentivirus-injected embryos.

In vitro lentivirus infection

Cultured keratinocytes were infected as previously described (Beronja et al., 2010). Briefly, keratinocytes were plated at 10^5 cells/well in six-well plates and infected with ∼10^7 colony-forming units of the appropriate lentiviruses encoding control (*shScr;puromycin or shScr;H2B-GFP*) or gene-specific shRNA in the presence of 100 µg/ml Polybrene (Sigma-Aldrich).

For Western blot and cell proliferation analyses, cultured keratinocytes were infected with *shScr;puromycin* (control) or gene-specific *shRNA;puromycin*. 48 h after infection, cells were selected with 2 µg/ml puromycin (Sigma-Aldrich) for an additional 72 h and then processed (see below). Keratinocytes were cultured in 50 µM Ca^{2+}; 24 h before harvesting, Ca^{2+} levels were increased to 300 µM. For differentiation assays, cultured keratinocytes were switched into 1.5 mM Ca^{2+} for 96 h and then analyzed.

Antibodies, immunofluorescence microscopy, and Western blotting

The following primary antibodies were used: stable β-catenin (05-665, 1:1,000), Millipore; occludin (ab31721, 1:100), ARP3 (ab49671, 1:500), Ki67 (ab15580, 1:300), GFP (ab13970, 1:2,000), BrdU (ab6326, 1:200), and SOX2 (ab97959 1:500), Abcam; β-catenin (610154, 1:800), integrin β4 (553745, 1:200), and CD-45 (553077, 1:100), BD Biosciences; ABI1 (39444, 1:1,000), phosphohistone H3 (3377, 1:800), survivin (2808, 1:500), Wave2 (3659, 1:400), SOX9 (82630, 1:300), stable β-catenin (19807, 1:800), Lef1 (2230, 1:800), and pGSK3β (9336, 1:1,000), Cell Signaling Technology; filaggrin (PRB-417P, 1:500), keratin 10 (PRB-159P, 1:1,000), keratin 14 (PRB-155P, 1:1,000), and pericentrin (PRB-432C, 1:500), Covance/BioLegend; P-cadherin (132000Z, 1:800) and ZO-1 (61-7300, 1:2,000), Invitrogen; desmoplakin (sc-33555, 1:750), nidogen (sc-33706, 1:2,000), and GSK3β (sc-53931, 1:500), Santa Cruz Biotechnology; and α-catenin (C8114, 1:1,000), Sigma-Aldrich.

Secondary antibodies were of the appropriate species/isotype reactivity conjugated to Alexa Fluor 488 or 647 or Rhodamine Red-X (Jackson ImmunoResearch). F-actin was labeled with phalloidin–Alexa Fluor 555 (8953; Cell Signaling Technology). Nuclei were labeled with DAPI (Sigma-Aldrich).

For immunofluorescence microscopy, the entire embryo was embedded in OCT compound (Scigen) and frozen. Skin sections (10 µm thick) were fixed for 10 min in 4% formaldehyde and blocked with PBS containing 0.3% Triton X-100, 1% BSA, 5% normal goat serum, 5% normal donkey serum, or MOM Basic kit (Vector Labs). Sections were incubated overnight at 4°C with primary antibodies at the dilutions described above. After washing, sections were incubated with the appropriate secondary antibody (1:1,500 dilution) at room temperature for 1 h. Images were acquired using a Nikon C2+ laser-scanning confocal microscope with a 60×/1.4 oil objective or a 20×/0.75 air objective (Nikon). Images were recorded at 1024 × 1024 square pixels. RGB images were assembled with ImageJ software (National Institutes of Health), and figure panels were labeled in Adobe Illustrator CS5, v.15.0.2.

For Western blotting, cells were lysed with RIPA buffer (Sigma-Aldrich), and proteins were quantified using a BCA kit (Pierce). Samples equivalent to 20–40 µg protein were resolved by 12% PAGE and electrotransferred to nitrocellulose membranes. Membranes were incubated overnight in a blocking solution (Tris-buffered saline, 0.3% Tween 20, and 5% nonfat milk) and then incubated with primary antibodies (1:1,000 dilution in blocking solution) overnight at 4°C. After washing, the membranes were incubated with HRP-conjugated antibodies (1:10,000 dilution in blocking solution) at room temperature for 1 h. The blots were developed using an Enhanced Chemiluminescence Detection Kit (Biological Industries) according to the manufacturer's instructions. Membrane images were obtain using FUSION FX7 spectra or Chemidoc Touch imaging systems.

Semiquantitative RT-PCR

Total RNA was extracted from primary epidermal keratinocytes using Direct-zol (Zymo Research; R2060). Equal amounts of RNA were reverse transcribed using ProtoScript First Strand cDNA Synthesis Kit (New England Biolabs), and semiquantitative PCR was conducted with a StepOnePlus System (Thermo Fisher Scientific). Reactions were performed using the indicated primers and cDNA template mixed with the LightCycler DNA Master SYBR Green mix and amplified for 40 cycles. The specificity of the reactions was determined by subsequent melting curve analysis. StepOnePlus analysis software was used to adjust for background fluorescence. The number of cycles needed to reach the crossing point for each sample was used to quantify each product using the 2–CP method. Data are presented as mRNA levels normalized to peptidylprolyl isomerase B (*Ppib*) mRNA levels.

Semi-quantitative RT-PCR primers were as follows: Abi1, forward 5′-TGGAGGTCCACTTTATTCTCAAA-3′ and reverse 5′-CCTGTGAGAGGGATCTGTGG-3′; Ccnd1, forward 5′-TTTCTTTCCAGAGTCATCAAGTGT-3′ and reverse 5′-TGACTCCAGAAGGGCTTCAA-3′; Jag1, forward 5′-TGGCCGAGGTCCTACACTT-3′ and reverse 5′-GCCTTTTCAATTATGCTATCAGG-3′; Lef1, forward 5′-CCGAAGAGGAAGGCGATTTAGCT-3′ and reverse 5′-GCTCCTGAGAGGTTTGTGCTTGTCT-3′; Ephb2, forward 5′-ACCCACTGTCCCATCAACAG-3′ and reverse 5′-CGTTGCGGCATACACAGTT-3′; Axin2, forward 5′-AGGAACCACTCGGCTGCT-3′ and reverse 5′-CAGTTTCTTTGGCTCTTTGTGA-3′; Bmp4, forward

5′-GAGGAGTTTCCATCACGAAGA-3′ and reverse 5′-GCTCTGCCG AGGAGATCA-3′; Wasf2, forward 5′-GGCTCATCCATTCACAGCA-3′ and reverse 5′-CAGGCGAGGTTCTCAATGAT-3′; and Ppib, forward 5′-GTGAGCGCTTCCCAGATGAGA-3′ and reverse 5′-TGC CGGAGTCGACAATGATG-3′.

Semiquantitative RT-PCR of Wnt targets

For semiquantitative RT-PCR of Wnt targets, cells were infected with *shScr;H2B-GFP* or *shAbi-2082*; *H2B-GFP*. Cells were treated with 10 ng Wnt3a (R&D Systems) 60 h after infection. Cells were processed 72 h after infection (see below).

BrdU/EdU incorporation assay and quantification of cell proliferation

Quantification of cell proliferation was performed as previously described (Luxenburg et al., 2015). Briefly, pregnant females were injected with the appropriate lentiviruses on E9, as described above. On E16.5, mice were injected with 25 mg/kg body weight of EdU or BrdU for 2 h, after which the embryos were collected, frozen in OCT, sectioned (10 µm thick), and fixed in 4% PFA. For BrdU staining, sections were then immersed in 4% HCl for an additional 40 min. For EdU staining, sections were incubated for 30 min in a solution containing copper sulfate, sulfo-cyanine 3 azide (2 µM; D1330; Lumiprobe), and sodium ascorbate (100 mM; Acros; 352685000).

Sections were imaged by confocal fluorescence microscopy, and the number of GFP^+, $BrdU^+$, and/or EdU^+ cells was counted. The percentage proliferating cells was calculated as ([number of EdU^+GFP^+ or $BrdU^+GFP^+$ double-positive cells])/total number of GFP^+ cells) × 100.

In vitro cell cycle analysis

Keratinocytes were infected with *shScr;puromycin* (control) and gene-specific shRNA;*puromycin*. Cells were pulsed for 3 h with 5 µM EdU, harvested, and stained for DAPI and EdU as described above. Cell cycle was analyzed using CytoFLEX FACS system and results were analyzed in cyteExprt software. Cells were gated for single-cell events, using SSC and DAPI channels. For Wnt inhibitor experiments, 5 µM XAV-939 (Sigma-Aldrich; X3004) was added 24 h before analysis.

Quantification of cortical F-actin staining intensity

Embryos of pregnant females were injected with lentiviruses harboring *shScr* or *shAbi1* on E9 and harvested at E16.5. Embryos were frozen in OCT, sectioned (10 µm), fixed, and incubated with Alexa Fluor 555–conjugated phalloidin (1:500) overnight at 4°C. F-actin staining was imaged using a Nikon C2+/60×/1.4 objective that generates optical sections of 0.49 µm. In mosaic patches, the fluorescence intensity of infected (GFP^+) and uninfected (GFP^-) basal and spinous layer cells was analyzed using the ImageJ line tool, and the ratio of $phalloidin^+GFP^+$ and $phalloidin^+GFP^-$ cells within the same field was calculated.

Quantification of active β-catenin

Embryos were injected with lentiviruses harboring *shScr* or *shAbi1* on E9 and harvested at E16.5. Embryos were frozen in OCT, sectioned (10 µm), fixed, and incubated with primary antibody against nonphospho β-catenin (1:800, 19807-CST) overnight at 4°C, and sections were incubated with secondary antibody at room temperature for 1 h. Staining was imaged using a Nikon C2+/40×/1.3 objective that generates optical sections of 0.69 µm. The fluorescence intensity of the cell cortex was measured using the ImageJ line tool in infected (GFP^+) spinous and granular layer cells.

Quantification of nuclear β-catenin fluorescence intensity

Cultured keratinocytes were treated with 125 nM latrunculin B (Sigma-Aldrich) or 250 nM jasplakinolide (Sigma-Aldrich) for 30 min, fixed, and stained for β-catenin, nonphospho β-catenin, and DNA (DAPI). Using NIS-elements AR software, the DAPI channel was used for automated object counting, then the mean intensity of β-catenin fluorescence was measured within the objects area and statistically analyzed.

Statistical analysis

Quantitative data are presented as the mean and standard deviation. Group differences were analyzed using an unpaired *t* test in Excel (Microsoft) or Prism (GraphPad). Sample sizes are indicated in the figure legends.

Online supplemental material

Fig. S1 shows that the Abi1-2082 depletion phenotype can be recapitulated by a second shRNA (Abi1-488) and rescued by coexpression of shRNA-resistant ABI1-GFP. Fig. S2 shows that Abi1-depleted epidermis exhibits normal localization of dermal papilla and normal number of $CD45^+$ cells. Fig. S3 shows that Abi1-depleted epidermis and cultured keratinocytes exhibit normal differentiation. Fig. S4 shows that Wasf2 KD by shWasf2-493 or shWasf2-269 phenocopies the epidermal defects induced by Abi1 depletion. Fig. S5 shows that Abi1-depleted epidermis exhibits non–cell autonomous phenotype. Fig. S6 shows that Abi1-depleted epidermis exhibits normal cell–cell adhesion structures.

Acknowledgments

We thank R. Zaidel-Bar, A. R. Folgueras, L. Broday, and R. Rosin-Arbesfeld for discussions and critical reading of the manuscript; R. Rosin-Arbesfeld and M. Caspi for technical assistance; and A. Vituri from the Statistical Laboratory, School of Mathematical Sciences, for help with statistical analysis.

This work was carried out in partial fulfillment of the requirements for the PhD degree for Y. Cohen and K. Padmanabhan and MSc degree for A. Soffer from the Sackler Faculty of Medicine, Tel Aviv University.

This work was supported by grants to C. Luxenburg from the Israel Science Foundation (number 1113/15) and the Israeli Centers for Research Excellence (I-CORE) Gene Regulation in Complex Human Disease (center number 41/11).

The authors declare no competing financial interests.

Author contributions: Y. Cohen conducted the experiments, collected and analyzed the data, and prepared the figures. S. Raviv identified *Abi1* shRNAs and prepared and injected the *shAbi1* lentivirus. O. Adir identified *Wasf2* shRNAs and prepared

and injected the *shWasf2* lentivirus. K. Padmanabhan and A. Soffer conducted viral work. C. Luxenburg and Y. Cohen designed the experiments and wrote the manuscript. C. Luxenburg supervised the study.

Submitted: 30 July 2018
Revised: 11 December 2018
Accepted: 1 February 2019

References

Ahtiainen, L., S. Lefebvre, P.H. Lindfors, E. Renvoisé, V. Shirokova, M.K. Vartiainen, I. Thesleff, and M.L. Mikkola. 2014. Directional cell migration, but not proliferation, drives hair placode morphogenesis. *Dev. Cell.* 28:588–602. https://doi.org/10.1016/j.devcel.2014.02.003

Alekhina, O., E. Burstein, and D.D. Billadeau. 2017. Cellular functions of WASP family proteins at a glance. *J. Cell Sci.* 130:2235–2241. https://doi.org/10.1242/jcs.199570

Amin, E., B.N. Dubey, S.C. Zhang, L. Gremer, R. Dvorsky, J.M. Moll, M.S. Taha, L. Nagel-Steger, R.P. Piekorz, A.V. Somlyo, and M.R. Ahmadian. 2013. Rho-kinase: regulation, (dys)function, and inhibition. *Biol. Chem.* 394:1399–1410. https://doi.org/10.1515/hsz-2013-0181

Amit, S., A. Hatzubai, Y. Birman, J.S. Andersen, E. Ben-Shushan, M. Mann, Y. Ben-Neriah, and I. Alkalay. 2002. Axin-mediated CKI phosphorylation of beta-catenin at Ser 45: a molecular switch for the Wnt pathway. *Genes Dev.* 16:1066–1076. https://doi.org/10.1101/gad.230302

Benitah, S.A., M. Frye, M. Glogauer, and F.M. Watt. 2005. Stem cell depletion through epidermal deletion of Rac1. *Science.* 309:933–935. https://doi.org/10.1126/science.1113579

Beronja, S., G. Livshits, S. Williams, and E. Fuchs. 2010. Rapid functional dissection of genetic networks via tissue-specific transduction and RNAi in mouse embryos. *Nat. Med.* 16:821–827. https://doi.org/10.1038/nm.2167

Beronja, S., P. Janki, E. Heller, W.H. Lien, B.E. Keyes, N. Oshimori, and E. Fuchs. 2013. RNAi screens in mice identify physiological regulators of oncogenic growth. *Nature.* 501:185–190. https://doi.org/10.1038/nature12464

Bisi, S., A. Disanza, C. Malinverno, E. Frittoli, A. Palamidessi, and G. Scita. 2013. Membrane and actin dynamics interplay at lamellipodia leading edge. *Curr. Opin. Cell Biol.* 25:565–573. https://doi.org/10.1016/j.ceb.2013.04.001

Blanpain, C., and E. Fuchs. 2009. Epidermal homeostasis: a balancing act of stem cells in the skin. *Nat. Rev. Mol. Cell Biol.* 10:207–217. https://doi.org/10.1038/nrm2636

Bubb, M.R., A.M. Senderowicz, E.A. Sausville, K.L. Duncan, and E.D. Korn. 1994. Jasplakinolide, a cytotoxic natural product, induces actin polymerization and competitively inhibits the binding of phalloidin to F-actin. *J. Biol. Chem.* 269:14869–14871.

Campellone, K.G., and M.D. Welch. 2010. A nucleator arms race: cellular control of actin assembly. *Nat. Rev. Mol. Cell Biol.* 11:237–251. https://doi.org/10.1038/nrm2867

Choi, Y.S., Y. Zhang, M. Xu, Y. Yang, M. Ito, T. Peng, Z. Cui, A. Nagy, A.K. Hadjantonakis, R.A. Lang, et al. 2013. Distinct functions for Wnt/β-catenin in hair follicle stem cell proliferation and survival and interfollicular epidermal homeostasis. *Cell Stem Cell.* 13:720–733. https://doi.org/10.1016/j.stem.2013.10.003

Cui, M., W. Yu, J. Dong, J. Chen, X. Zhang, and Y. Liu. 2010. Downregulation of ABI1 expression affects the progression and prognosis of human gastric carcinoma. *Med. Oncol.* 27:632–639. https://doi.org/10.1007/s12032-009-9260-6

DasGupta, R., and E. Fuchs. 1999. Multiple roles for activated LEF/TCF transcription complexes during hair follicle development and differentiation. *Development.* 126:4557–4568.

Dor-On, E., S. Raviv, Y. Cohen, O. Adir, K. Padmanabhan, and C. Luxenburg. 2017. T-plastin is essential for basement membrane assembly and epidermal morphogenesis. *Sci. Signal.* 10:eaal3154. https://doi.org/10.1126/scisignal.aal3154

Driskell, R.R., C. Clavel, M. Rendl, and F.M. Watt. 2011. Hair follicle dermal papilla cells at a glance. *J. Cell Sci.* 124:1179–1182. https://doi.org/10.1242/jcs.082446

Dubielecka, P.M., K.I. Ladwein, X. Xiong, I. Migeotte, A. Chorzalska, K.V. Anderson, J.A. Sawicki, K. Rottner, T.E. Stradal, and L. Kotula. 2011. Essential role for Abi1 in embryonic survival and WAVE2 complex integrity. *Proc. Natl. Acad. Sci. USA.* 108:7022–7027. https://doi.org/10.1073/pnas.1016811108

Fuchs, E. 2007. Scratching the surface of skin development. *Nature.* 445:834–842. https://doi.org/10.1038/nature05659

Ghahramani, A., G. Donati, N.M. Luscombe, and F.M. Watt. 2018. Epidermal Wnt signalling regulates transcriptome heterogeneity and proliferative fate in neighbouring cells. *Genome Biol.* 19:3. https://doi.org/10.1186/s13059-017-1384-y

Guo, C., S. Liu, J. Wang, M.Z. Sun, and F.T. Greenaway. 2013. ACTB in cancer. *Clin. Chim. Acta.* 417:39–44. https://doi.org/10.1016/j.cca.2012.12.012

Guo, W., Z. Keckesova, J.L. Donaher, T. Shibue, V. Tischler, F. Reinhardt, S. Itzkovitz, A. Noske, U. Zürrer-Härdi, G. Bell, et al. 2012. Slug and Sox9 cooperatively determine the mammary stem cell state. *Cell.* 148:1015–1028. https://doi.org/10.1016/j.cell.2012.02.008

Hegde, S., and S. Raghavan. 2013. A skin-depth analysis of integrins: role of the integrin network in health and disease. *Cell Commun. Adhes.* 20:155–169. https://doi.org/10.3109/15419061.2013.854334

Heller, E., K.V. Kumar, S.W. Grill, and E. Fuchs. 2014. Forces generated by cell intercalation tow epidermal sheets in mammalian tissue morphogenesis. *Dev. Cell.* 28:617–632. https://doi.org/10.1016/j.devcel.2014.02.011

Innocenti, M., E. Frittoli, I. Ponzanelli, J.R. Falck, S.M. Brachmann, P.P. Di Fiore, and G. Scita. 2003. Phosphoinositide 3-kinase activates Rac by entering in a complex with Eps8, Abi1, and Sos-1. *J. Cell Biol.* 160:17–23. https://doi.org/10.1083/jcb.200206079

Innocenti, M., A. Zucconi, A. Disanza, E. Frittoli, L.B. Areces, A. Steffen, T.E. Stradal, P.P. Di Fiore, M.F. Carlier, and G. Scita. 2004. Abi1 is essential for the formation and activation of a WAVE2 signalling complex. *Nat. Cell Biol.* 6:319–327. https://doi.org/10.1038/ncb1105

Innocenti, M., S. Gerboth, K. Rottner, F.P. Lai, M. Hertzog, T.E. Stradal, E. Frittoli, D. Didry, S. Polo, A. Disanza, et al. 2005. Abi1 regulates the activity of N-WASP and WAVE in distinct actin-based processes. *Nat. Cell Biol.* 7:969–976. https://doi.org/10.1038/ncb1304

Jung, Y.S., W. Wang, S. Jun, J. Zhang, M. Srivastava, M.J. Kim, E.M. Lien, J. Shang, J. Chen, P.D. McCrea, et al. 2018. Deregulation of CRAD-controlled cytoskeleton initiates mucinous colorectal cancer via β-catenin. *Nat. Cell Biol.* 20:1303–1314. https://doi.org/10.1038/s41556-018-0215-z

Kadaja, M., B.E. Keyes, M. Lin, H.A. Pasolli, M. Genander, L. Polak, N. Stokes, D. Zheng, and E. Fuchs. 2014. SOX9: a stem cell transcriptional regulator of secreted niche signaling factors. *Genes Dev.* 28:328–341. https://doi.org/10.1101/gad.233247.113

Kalailingam, P., H.B. Tan, N. Jain, M.K. Sng, J.S.K. Chan, N.S. Tan, and T. Thanabalu. 2017. Conditional knock out of N-WASP in keratinocytes causes skin barrier defects and atopic dermatitis-like inflammation. *Sci. Rep.* 7:7311. https://doi.org/10.1038/s41598-017-07125-8

Kotula, L. 2012. Abi1, a critical molecule coordinating actin cytoskeleton reorganization with PI-3 kinase and growth signaling. *FEBS Lett.* 586:2790–2794. https://doi.org/10.1016/j.febslet.2012.05.015

Kurbet, A.S., S. Hegde, O. Bhattacharjee, S. Marepally, P.K. Vemula, and S. Raghavan. 2016. Sterile Inflammation Enhances ECM Degradation in Integrin β1 KO Embryonic Skin. *Cell Reports.* 16:3334–3347. https://doi.org/10.1016/j.celrep.2016.08.062

Larsimont, J.C., K.K. Youssef, A. Sánchez-Danés, V. Sukumaran, M. Defrance, B. Delatte, M. Liagre, P. Baatsen, J.C. Marine, S. Lippens, et al. 2015. Sox9 Controls Self-Renewal of Oncogene Targeted Cells and Links Tumor Initiation and Invasion. *Cell Stem Cell.* 17:60–73. https://doi.org/10.1016/j.stem.2015.05.008

Lee, N.K., K.W. Fok, A. White, N.H. Wilson, C.J. O'Leary, H.L. Cox, M. Michael, A.S. Yap, and H.M. Cooper. 2016. Neogenin recruitment of the WAVE regulatory complex maintains adherens junction stability and tension. *Nat. Commun.* 7:11082. https://doi.org/10.1038/ncomms11082

Lefever, T., E. Pedersen, A. Basse, R. Paus, F. Quondamatteo, A.C. Stanley, L. Langbein, X. Wu, J. Wehland, S. Lommel, and C. Brakebusch. 2010. N-WASP is a novel regulator of hair-follicle cycling that controls antiproliferative TGFbeta pathways. *J. Cell Sci.* 123:128–140. https://doi.org/10.1242/jcs.053835

Lian, G., M. Dettenhofer, J. Lu, M. Downing, A. Chenn, T. Wong, and V. Sheen. 2016. Filamin A- and formin 2-dependent endocytosis regulates proliferation via the canonical Wnt pathway. *Development.* 143:4509–4520. https://doi.org/10.1242/dev.139295

Lim, X., and R. Nusse. 2013. Wnt signaling in skin development, homeostasis, and disease. *Cold Spring Harb. Perspect. Biol.* 5:a008029. https://doi.org/10.1101/cshperspect.a008029

Lim, X., S.H. Tan, W.L. Koh, R.M. Chau, K.S. Yan, C.J. Kuo, R. van Amerongen, A.M. Klein, and R. Nusse. 2013. Interfollicular epidermal stem cells

self-renew via autocrine Wnt signaling. *Science.* 342:1226–1230. https://doi.org/10.1126/science.1239730

Luxenburg, C., and B. Geiger. 2017. Multiscale View of Cytoskeletal Mechanoregulation of Cell and Tissue Polarity. *Handb. Exp. Pharmacol.* 235: 263–284. https://doi.org/10.1007/164_2016_34

Luxenburg, C., H.A. Pasolli, S.E. Williams, and E. Fuchs. 2011. Developmental roles for Srf, cortical cytoskeleton and cell shape in epidermal spindle orientation. *Nat. Cell Biol.* 13:203–214. https://doi.org/10.1038/ncb2163

Luxenburg, C., E. Heller, H.A. Pasolli, S. Chai, M. Nikolova, N. Stokes, and E. Fuchs. 2015. Wdr1-mediated cell shape dynamics and cortical tension are essential for epidermal planar cell polarity. *Nat. Cell Biol.* 17: 592–604. https://doi.org/10.1038/ncb3146

Lyubimova, A., J.J. Garber, G. Upadhyay, A. Sharov, F. Anastasoaie, V. Yajnik, G. Cotsarelis, G.P. Dotto, V. Botchkarev, and S.B. Snapper. 2010. Neural Wiskott-Aldrich syndrome protein modulates Wnt signaling and is required for hair follicle cycling in mice. *J. Clin. Invest.* 120:446–456. https://doi.org/10.1172/JCI36478

Machesky, L.M., and K.L. Gould. 1999. The Arp2/3 complex: a multifunctional actin organizer. *Curr. Opin. Cell Biol.* 11:117–121. https://doi.org/10.1016/S0955-0674(99)80014-3

Machesky, L.M., S.J. Atkinson, C. Ampe, J. Vandekerckhove, and T.D. Pollard. 1994. Purification of a cortical complex containing two unconventional actins from Acanthamoeba by affinity chromatography on profilin-agarose. *J. Cell Biol.* 127:107–115. https://doi.org/10.1083/jcb.127.1.107

Machesky, L.M., R.D. Mullins, H.N. Higgs, D.A. Kaiser, L. Blanchoin, R.C. May, M.E. Hall, and T.D. Pollard. 1999. Scar, a WASp-related protein, activates nucleation of actin filaments by the Arp2/3 complex. *Proc. Natl. Acad. Sci. USA.* 96:3739–3744. https://doi.org/10.1073/pnas.96.7.3739

Miki, H., S. Suetsugu, and T. Takenawa. 1998. WAVE, a novel WASP-family protein involved in actin reorganization induced by Rac. *EMBO J.* 17: 6932–6941. https://doi.org/10.1093/emboj/17.23.6932

Miroshnikova, Y.A., H.Q. Le, D. Schneider, T. Thalheim, M. Rubsam, N. Bremicker, J. Polleux, N. Kamprad, M. Tarantola, I. Wang, et al. 2018. Adhesion forces and cortical tension couple cell proliferation and differentiation to drive epidermal stratification. *Nat. Cell Biol.* 20:69–80.

Morton, W.M., K.R. Ayscough, and P.J. McLaughlin. 2000. Latrunculin alters the actin-monomer subunit interface to prevent polymerization. *Nat. Cell Biol.* 2:376–378. https://doi.org/10.1038/35014075

Nowak, J.A., and E. Fuchs. 2009. Isolation and culture of epithelial stem cells. *Methods Mol. Biol.* 482:215–232. https://doi.org/10.1007/978-1-59745-060-7_14

Nowak, J.A., L. Polak, H.A. Pasolli, and E. Fuchs. 2008. Hair follicle stem cells are specified and function in early skin morphogenesis. *Cell Stem Cell.* 3: 33–43. https://doi.org/10.1016/j.stem.2008.05.009

Olson, E.N., and A. Nordheim. 2010. Linking actin dynamics and gene transcription to drive cellular motile functions. *Nat. Rev. Mol. Cell Biol.* 11: 353–365. https://doi.org/10.1038/nrm2890

Ouspenskaia, T., I. Matos, A.F. Mertz, V.F. Fiore, and E. Fuchs. 2016. WNT-SHH Antagonism Specifies and Expands Stem Cells prior to Niche Formation. *Cell.* 164:156–169. https://doi.org/10.1016/j.cell.2015.11.058

Paus, R., S. Müller-Röver, C. Van Der Veen, M. Maurer, S. Eichmüller, G. Ling, U. Hofmann, K. Foitzik, L. Mecklenburg, and B. Handjiski. 1999. A comprehensive guide for the recognition and classification of distinct stages of hair follicle morphogenesis. *J. Invest. Dermatol.* 113:523–532. https://doi.org/10.1046/j.1523-1747.1999.00740.x

Pollard, T.D., and J.A. Cooper. 2009. Actin, a central player in cell shape and movement. *Science.* 326:1208–1212. https://doi.org/10.1126/science.1175862

Pollitt, A.Y., and R.H. Insall. 2008. Abi mutants in Dictyostelium reveal specific roles for the SCAR/WAVE complex in cytokinesis. *Curr. Biol.* 18: 203–210. https://doi.org/10.1016/j.cub.2008.01.026

Raghavan, S., C. Bauer, G. Mundschau, Q. Li, and E. Fuchs. 2000. Conditional ablation of beta1 integrin in skin. Severe defects in epidermal proliferation, basement membrane formation, and hair follicle invagination. *J. Cell Biol.* 150:1149–1160. https://doi.org/10.1083/jcb.150.5.1149

Rhee, H., L. Polak, and E. Fuchs. 2006. Lhx2 maintains stem cell character in hair follicles. *Science.* 312:1946–1949. https://doi.org/10.1126/science.1128004

Ring, C., M.H. Ginsberg, J. Haling, and A.M. Pendergast. 2011. Abl-interactor-1 (Abi1) has a role in cardiovascular and placental development and is a binding partner of the alpha4 integrin. *Proc. Natl. Acad. Sci. USA.* 108: 149–154. https://doi.org/10.1073/pnas.1012316108

Riviere, J.B., B.W. van Bon, A. Hoischen, S.S. Kholmanskikh, B.J. O'Roak, C. Gilissen, S. Gijsen, C.T. Sullivan, S.L. Christian, O.A. Abdul-Rahman, et al. 2012. De novo mutations in the actin genes ACTB and ACTG1 cause Baraitser-Winter syndrome. *Nat. Genet.* 44:440–444.

Roberts, N., and V. Horsley. 2014. Developing stratified epithelia: lessons from the epidermis and thymus. *Wiley Interdiscip. Rev. Dev. Biol.* 3: 389–402. https://doi.org/10.1002/wdev.146

Rognoni, E., M. Widmaier, M. Jakobson, R. Ruppert, S. Ussar, D. Katsougkri, R.T. Böttcher, J.E. Lai-Cheong, D.B. Rifkin, J.A. McGrath, and R. Fässler. 2014. Kindlin-1 controls Wnt and TGF-β availability to regulate cutaneous stem cell proliferation. *Nat. Med.* 20:350–359. https://doi.org/10.1038/nm.3490

Rotty, J.D., C. Wu, and J.E. Bear. 2013. New insights into the regulation and cellular functions of the ARP2/3 complex. *Nat. Rev. Mol. Cell Biol.* 14: 7–12. https://doi.org/10.1038/nrm3492

Rubsam, M., J.A. Broussard, S.A. Wickstrom, O. Nekrasova, K.J. Green, and C. M. Niessen. 2018. Adherens junctions and desmosomes coordinate mechanics and signaling to orchestrate tissue morphogenesis and function: an evolutionary perspective. *Cold Spring Harb. Perspect. Biol.* 10:a029207.

Rübsam, M., A.F. Mertz, A. Kubo, S. Marg, C. Jüngst, G. Goranci-Buzhala, A.C. Schauss, V. Horsley, E.R. Dufresne, M. Moser, et al. 2017. E-cadherin integrates mechanotransduction and EGFR signaling to control junctional tissue polarization and tight junction positioning. *Nat. Commun.* 8:1250. https://doi.org/10.1038/s41467-017-01170-7

Ryu, J.R., A. Echarri, R. Li, and A.M. Pendergast. 2009. Regulation of cell-cell adhesion by Abi/Diaphanous complexes. *Mol. Cell. Biol.* 29:1735–1748. https://doi.org/10.1128/MCB.01483-08

Samuel, M.S., J.I. Lopez, E.J. McGhee, D.R. Croft, D. Strachan, P. Timpson, J. Munro, E. Schröder, J. Zhou, V.G. Brunton, et al. 2011. Actomyosin-mediated cellular tension drives increased tissue stiffness and β-catenin activation to induce epidermal hyperplasia and tumor growth. *Cancer Cell.* 19:776–791. https://doi.org/10.1016/j.ccr.2011.05.008

Sasidharan, S., S. Borinskaya, F. Patel, Y. Bernadskaya, S. Mandalapu, M. Agapito, and M.C. Soto. 2018. WAVE regulates Cadherin junction assembly and turnover during epithelial polarization. *Dev. Biol.* 434: 133–148. https://doi.org/10.1016/j.ydbio.2017.12.002

Schlegelmilch, K., M. Mohseni, O. Kirak, J. Pruszak, J.R. Rodriguez, D. Zhou, B.T. Kreger, V. Vasioukhin, J. Avruch, T.R. Brummelkamp, and F.D. Camargo. 2011. Yap1 acts downstream of α-catenin to control epidermal proliferation. *Cell.* 144:782–795. https://doi.org/10.1016/j.cell.2011.02.031

Shi, G., K.C. Sohn, Z. Li, D.K. Choi, Y.M. Park, J.H. Kim, Y.M. Fan, Y.H. Nam, S. Kim, M. Im, et al. 2013. Expression and functional role of Sox9 in human epidermal keratinocytes. *PLoS One.* 8:e54355. https://doi.org/10.1371/journal.pone.0054355

Shi, Y., K. Alin, and S.P. Goff. 1995. Abl-interactor-1, a novel SH3 protein binding to the carboxy-terminal portion of the Abl protein, suppresses v-abl transforming activity. *Genes Dev.* 9:2583–2597. https://doi.org/10.1101/gad.9.21.2583

Silvis, M.R., B.T. Kreger, W.H. Lien, O. Klezovitch, G.M. Rudakova, F.D. Camargo, D.M. Lantz, J.T. Seykora, and V. Vasioukhin. 2011. α-catenin is a tumor suppressor that controls cell accumulation by regulating the localization and activity of the transcriptional coactivator Yap1. *Sci. Signal.* 4:ra33. https://doi.org/10.1126/scisignal.2001823

Simpson, C.L., D.M. Patel, and K.J. Green. 2011. Deconstructing the skin: cytoarchitectural determinants of epidermal morphogenesis. *Nat. Rev. Mol. Cell Biol.* 12:565–580. https://doi.org/10.1038/nrm3175

Steinestel, K., S. Brüderlein, J.K. Lennerz, J. Steinestel, K. Kraft, C. Pröpper, V. Meineke, and P. Möller. 2014. Expression and Y435-phosphorylation of Abelson interactor 1 (Abi1) promotes tumour cell adhesion, extracellular matrix degradation and invasion by colorectal carcinoma cells. *Mol. Cancer.* 13:145. https://doi.org/10.1186/1476-4598-13-145

Stradal, T.E., K. Rottner, A. Disanza, S. Confalonieri, M. Innocenti, and G. Scita. 2004. Regulation of actin dynamics by WASP and WAVE family proteins. *Trends Cell Biol.* 14:303–311. https://doi.org/10.1016/j.tcb.2004.04.007

Sun, X., C. Li, C. Zhuang, W.C. Gilmore, E. Cobos, Y. Tao, and Z. Dai. 2009. Abl interactor 1 regulates Src-Id1-matrix metalloproteinase 9 axis and is required for invadopodia formation, extracellular matrix degradation and tumor growth of human breast cancer cells. *Carcinogenesis.* 30: 2109–2116. https://doi.org/10.1093/carcin/bgp251

van der Kammen, R., J.Y. Song, I. de Rink, H. Janssen, S. Madonna, C. Scarponi, C. Albanesi, W. Brugman, and M. Innocenti. 2017. Knockout of the Arp2/3 complex in epidermis causes a psoriasis-like disease hallmarked by hyperactivation of transcription factor Nrf2. *Development.* 144: 4588–4603. https://doi.org/10.1242/dev.156323

Veltri, A., C. Lang, and W.H. Lien. 2018. Concise Review: Wnt signaling pathways in skin development and epidermal stem cells. *Stem Cells.* 36: 22–35.

Vidal, V.P., M.C. Chaboissier, S. Lützkendorf, G. Cotsarelis, P. Mill, C.C. Hui, N. Ortonne, J.P. Ortonne, and A. Schedl. 2005. Sox9 is essential for outer root sheath differentiation and the formation of the hair stem cell compartment. *Curr. Biol.* 15:1340–1351. https://doi.org/10.1016/j.cub.2005.06.064

Vidal, V.P., N. Ortonne, and A. Schedl. 2008. SOX9 expression is a general marker of basal cell carcinoma and adnexal-related neoplasms. *J. Cutan. Pathol.* 35:373–379. https://doi.org/10.1111/j.1600-0560.2007.00815.x

Wang, T., R.A. Cleary, R. Wang, and D.D. Tang. 2013. Role of the adapter protein Abi1 in actin-associated signaling and smooth muscle contraction. *J. Biol. Chem.* 288:20713–20722. https://doi.org/10.1074/jbc.M112.439877

Wei, L., M. Surma, S. Shi, N. Lambert-Cheatham, and J. Shi. 2016. Novel Insights into the Roles of Rho Kinase in Cancer. *Arch. Immunol. Ther. Exp. (Warsz.).* 64:259–278. https://doi.org/10.1007/s00005-015-0382-6

Welch, M.D., A.H. DePace, S. Verma, A. Iwamatsu, and T.J. Mitchison. 1997. The human Arp2/3 complex is composed of evolutionarily conserved subunits and is localized to cellular regions of dynamic actin filament assembly. *J. Cell Biol.* 138:375–384. https://doi.org/10.1083/jcb.138.2.375

Williams, S.E., S. Beronja, H.A. Pasolli, and E. Fuchs. 2011. Asymmetric cell divisions promote Notch-dependent epidermal differentiation. *Nature.* 470:353–358. https://doi.org/10.1038/nature09793

Winter, D., A.V. Podtelejnikov, M. Mann, and R. Li. 1997. The complex containing actin-related proteins Arp2 and Arp3 is required for the motility and integrity of yeast actin patches. *Curr. Biol.* 7:519–529. https://doi.org/10.1016/S0960-9822(06)00223-5

Wu, X., F. Quondamatteo, T. Lefever, A. Czuchra, H. Meyer, A. Chrostek, R. Paus, L. Langbein, and C. Brakebusch. 2006. Cdc42 controls progenitor cell differentiation and beta-catenin turnover in skin. *Genes Dev.* 20: 571–585. https://doi.org/10.1101/gad.361406

Xiong, X., A. Chorzalska, P.M. Dubielecka, J.R. White, Y. Vedvyas, C.V. Hedvat, A. Haimovitz-Friedman, J.A. Koutcher, J. Reimand, G.D. Bader, et al. 2012. Disruption of Abi1/Hssh3bp1 expression induces prostatic intraepithelial neoplasia in the conditional Abi1/Hssh3bp1 KO mice. *Oncogenesis.* 1:e26. https://doi.org/10.1038/oncsis.2012.28

Zaidel-Bar, R., G. Zhenhuan, and C. Luxenburg. 2015. The contractome--a systems view of actomyosin contractility in non-muscle cells. *J. Cell Sci.* 128:2209–2217. https://doi.org/10.1242/jcs.170068

Zhang, H., H.A. Pasolli, and E. Fuchs. 2011. Yes-associated protein (YAP) transcriptional coactivator functions in balancing growth and differentiation in skin. *Proc. Natl. Acad. Sci. USA.* 108:2270–2275. https://doi.org/10.1073/pnas.1019603108

Zhou, K., A. Muroyama, J. Underwood, R. Leylek, S. Ray, S.H. Soderling, and T. Lechler. 2013. Actin-related protein2/3 complex regulates tight junctions and terminal differentiation to promote epidermal barrier formation. *Proc. Natl. Acad. Sci. USA.* 110:E3820–E3829. https://doi.org/10.1073/pnas.1308419110